Investigation of All-Optical Clock Recovery Methods

A Project Report

submitted by

Lunavath Mahesh

in partial fulfilment of requirements

for the award of the degree of

MASTER OF TECHNOLOGY

DEPARTMENT OF ELECTRICAL ENGINEERING

INDIAN INSTITUTE OF TECHNOLOGY MADRAS

JUNE 2017

THESIS CERTIFICATE

This is to certify that the thesis titled **Investigation of All-Optical Clock Recovery Methods**, submitted by **Lunavath Mahesh**, to the Indian Institute of Technology Madras, Chennai for the award of the degree of **Master of Technology (Photonics) in Electrical Engineering Department**, is a bonafide record of the research work done by him under my supervision. The contents of this thesis, in full or in parts, have not been submitted to any other Institute or University for the award of any degree or diploma.

Prof. R. Manivasakan
Research Guide
Assistant Professor
Dept. of Electrical Engineering
IIT Madras - 600036

Place: Chennai

Date: 4th June 2017

ACKNOWLEDGEMENTS

First of all I would like to thank Prof. R. Manivasakan for his supervision, valuable advices throughout this work. I have appreciated his friendly personality and the patience with which he answers my questions, no matter how simple they may be.

I would like to thank Prof. Deepa Venkitesh. I have gained a great knowledge in nonlinear optics from her course on optical signal processing and she was a source of inspiration to me personally. I would also like to thank Prof. Balaji Srinivasan. I have benefited from his knowledge both as a student, and also as a teaching assistant in his course. I am grateful to all the professors of Photonics group (EE5) of Department of Electrical for their support and encouragement.

Special thanks to my friend Lakshmi Narayanan who was a constant source of support and motivation for me during my difficulty times. Also I am thankful to all my fellow batch mates who made my days spent in this college so memorable and colorful. I would like to mention students and researchers in Photonics lab who have befriended me and supported me along the way.

Finally, I would like to thank my family especially my brother for his constant love, support and guidance.

ABSTRACT

KEYWORDS: Optical Clock Recovery, Phase Lock Loop, Injection Locking, Mode Locked Lasers, Fabry-Perot Filter

The recent increase of internet traffic is creating demand for higher bandwidth in telecommunication networks. In order to satisfy this ever increasing demand for bandwidth, it is necessary to investigate new devices and technologies for all-optical signal processing that allow increasing the transmission data rate and the capacity for the current and future optical networks. Optical time division multiplexing (OTDM) is a widely deployed technique that allows increasing the bit rate and capacity of optical networks. In OTDM networks the regeneration and the demultiplexing of the data channels are two common and important functions normally carried out. However, they require a clock signal, which is usually implemented by optoelectronics components, making a system expensive, bulky and difficult to implement. In order to provide a solution to this issue, the focus of this thesis is to investigate all-optical clock recovery techniques. Clock recovery, is one of the most important tasks at network nodes and receivers as it allows synchronous signal processing operations, which usually yield a high performance.

In this report optical clock recovery methods are investigated and studied in detail. Numerical models are designed for each of the methods. A technique for all optical timing extraction and clock recovery is presented using SOA as phase comparator in PLL configuration. For the filtering model a Fabry-Perot Filter is used and pattern sequence dependence on the clock recovery model is computed using a novel remodulation technique to characterize the clock recovery system. A brief theory for CW Injection Locking and Pulsed Injection locking of mode locked lasers is presented. The variations of temporal and spectral characteristics of a monolithic mode locked laser under injection locking condition were qualitatively explained with a simple numerical model.

TABLE OF CONTENTS

ACKNOWLEDGEMENT **i**

ABSTRACT **ii**

LIST OF FIGURES **v**

1. INTRODUCTION **1**

1.1. Background and Motivation……..……..... 1

1.2. Role of Clock Recovery in Optical Networks…….. 2

1.3. Optical Clock Recovery Methods……..……... 2

1.4. Conclusion ……..……...……... 6

2. OPTICAL PHASE LOCK LOOP METHOD **7**

2.1. Introduction……..…….……..... 7

2.2. Optical Clock Recovery using SOA……...…….. 7

2.2.1. Pulse Propagation in SOA…… 8

2.2.2. All Optical timing Extraction…… 9

2.2.3. Error Signal Generation…… 11

2.2.4. Clock Recovery System…….....…… 13

2.2.5. Numerical Model……..…… 14

2.2.6. Simulation Results…….…... 16

2.3. Conclusion……..……. . 19

3. FILTERING METHOD **20**

3.1. Introduction……..…….……..... 20

3.2. Optical resonators……..…….. 20

3.3. Optical Clock Recovery using Fabry-Perot Filter……...…...……... 22

3.3.1. Simulation Setup……...…….... 23

3.3.2. Remodulation Technique……..…….... 24

3.3.3. Simulation Results…….…... 26

3.4. Conclusion……..……... 28

4. INJECTION LOCKING METHOD 29

4.1. CW Injection Locking Theory……..……..... 29

4.1.1. Diagnostic for Injection locking……...…….…... 33

4.2. Mode Locked Laser Fundamentals…….. 34

4.3. Pulsed Coherent Injection Locking of Mode Locked Laser……..……. . 37

4.4. Numerical Model…….. 40

4.4.1. Simulation Results…….…...…….…... 45

4.5. Conclusion……..…….. 49

BIBLIOGRAPHY 50

LIST OF FIGURES

1.1 Schematic representation of a PLL in CR setup……..3

1.2 Operation principle of an Optical CR based on spectral line filtering technique…5

2.1 Typical Optical Phase Lock Loop……7

2.2 Time dependent gain of an SOA with 3ps FWHM input pulse for Gain=20 (a) Real case (b) Ideal case …….……8

2.3 (a) Schematic configuration of all-optical timing extraction) Idealistic SOA output pulses for delay of +2ps and -2ps (c)The Ideal SOA simulated transmitted peak power from each output as a function of timing delay between the two pulses inside the wave-guide……10

2.4 (a)Schematic for error signal generation (b)Simulated error signal versus time with an open loop feedback. The frequency difference between the data and clock is 10 kHz, LPF Bandwidth ≅ 15 kHz……12

2.5 Simulation setup for optical clock recovery system……..13

2.6 Schematic configuration of PLL open loop feedback……15

2.7 The simulated transient response of the error signal using SOA with a $2^7 - 1$ PRBS data, running at (a)10Gbit/s (b)40Gbit/s (c)160Gbit/s, LPF BW≈100MHz,$\Delta f = 1$MHz……...17

2.9 The simulated timing jitter as function of different data bit rates……..19

3.1 Illustration of pulse propagation in Fabry-Perot Resonator……...21

3.2 (a) The Transmitted Intensity (b) Reflectivity Finesse versus Mirror Reflectivity R of a Fabry-Perot Resonator……22

3.3 All-Optical clock recovery setup using Filtering Method…….23

3.4 Setup of the remodulation technique used to study RCK quality…….24

3.5 EOF Vs Finesse for the FPF alone case…….26

3.6 Eye opening factor Vs Fabry-Perot Filter finesse for $2^7 - 1$ bits/seq …….27

3.7 EOF vs Finesse for FPF + SOA output remodulated ……27

4.1 Schematic model for Injection Locking…….30

4.2 Phase difference $\phi_1 - \phi$ between the injected wave and the injection locked laser output wave, for several values of the power ratio $P_{inc,refl}/P_{out}$……....32

4.3 Resonant cavity modes and gain spectrum of a laser (a) for single mode lasing (b) for multimode lasing……..35

4.4 Simulation of mode locking. In this simulation, the cavity has FSR = 100 MHz (a) No phase coherence between the multiple modes (80 modes simulated) (b) 5 phase coherent modes (c) 80 phase coherent modes…….36

4.5 Illustration of optically driven active mode locking……..38

4.6 Illustration of Pulsed coherent injection locking……...39

4.7 Schematic of numerical model for pulsed injection locking of a mode locked laser……40

4.8 Simulated reflected power from the laser cavity……...45

4.9 Simulated laser spectra for various values of θ…….46

4.10 Selected simulated laser output spectra, for values of θ within the coherent locking range. A shift in the peak of the spectrum occurs as θ is tune…….49

4.11 Simulated laser pulses for various values of θ……..…48

4.12 Selected simulated laser pulses for values of θ within the coherent injection locking range…….48

CHAPTER 1

INTRODUCTION

1.1 Background and Motivation

A great interest has been developed in optical communication field in recent years, especially after the remarkable advances in the technologies of lasers and optical fibers. Transmission of data along optical fibers for long distances result in data degradation and distortion due to the optical fiber impairments such as Kerr nonlinearities and chromatic dispersion, in addition to accumulated amplified spontaneous emission noise through cascaded optical amplifier stages. Currently deployed systems of signal processing use optical-electrical-optical (O-E-O) technology. In this approach, the optical data is detected and converted into an electrical signal for electronic processing. The processed data is then converted into optical signal using electrical/optical converters in order to retransmit along optical fiber. This conversion process is limited by the speed of electronic components, which represents a bottleneck for high-speed optical processing that supposed to function at high data rates. Therefore, the use of optical signal repeaters and regenerators at periodic transmission distances is desirable to re-amplify, re-shape, and re-time the transmitted data bits. This way longer transmission distances can be reached with an error free operation. The 3R regeneration is used to overcome all these signal degradations by associating a 2R device with a retiming function. 3R regenerators with retiming capability require clock extraction from the incoming data signal. The capacity demand growth of optical networks is irresistible and will reach electronic limitations. Furthermore, all-optical solutions offer a transparency for the optical networks. All-Optical Clock Recovery (CR) is one of the principal sub-functions of a full all-optical 3R regenerator.

1.2 Role of Clock Recovery in Optical Networks

In optical networks, clock recovery is a key function among the functional blocks such as receiver, in-line repeaters and demultiplexers in future OTDM systems. The role of the Clock Recovery (CR) function in these elements is extracting a stable clock which is synchronized (in frequency and in phase) to the incoming data signal and ideally with a minimal timing jitter.

In a receiver, CRs provide a time reference to the decision gate. Decision of value 0 or 1 of a bit is made at an accurate moment. The decisions have to be done in a regular rhythm, and duration between two successive decisions has to be equal to the bit duration. If the repetition rates of the data signal and of the clock are different, the decision moment slips step by step far away from the optimal sampling time. This deviation introduces errors and the detection gives false information. Therefore the clock which is used for receiver time reference must be derived accurately from the received signal itself. In future OTDM systems, temporal demultiplexing requires a CR to extract a base rate clock B/N from a transmitted OTDM data signal which is at a line rate B. The CR must provide a low timing jitter clock which is synchronized to the incoming data signal. Afterwards, the recovered clock is distributed to demultiplexers, routers, channel selectors, and receivers. In OTDM systems, the aggregate data rate exceeds the state-of-the-art speed limit of electronic components, all-optical CR offers a novel solution to provide retiming signals and perform. The first advantage of the optical solution is the transparency for optical networks. The second advantage is that optical CRs allow operation at ultrahigh bit rates which could not be achieved by using only optoelectronic components.

1.3 Optical Clock Recovery Methods

A broad variety of concepts and implementations have been proposed for all-optical clock recovery. We can classify CR techniques in three categories according to their operating principles [T. von Lerber 2009][2].

1. Phase-Locked Loop Method (PLL)
2. Spectral Filtering Method

3. Self-Pulsating Lasers (Injection Locking)

For each technique, there are also a lot of sophisticated approaches which exploit optoelectronic components only, optical components only, or mixing of both.

Phase-locked loop Method

A phase locked loop (PLL) is a control system in a closed-loop that generates an output signal in relation to the frequency and phase of a reference input signal. The PLL consists basically of a phase detector, a low-pass filter and a voltage-controlled oscillator (VCO). An example of a very simple PLL is depicted in Fig.1.1. The phase-locked loop circuit responds to the input signal by automatically adjusting the frequency of the controlled oscillator until it is matched to the frequency of the reference signal. In general, parameters of amplification and filtering stages determine the loop operating range, the locking characteristics and the residual phase mismatch between input and output signals. Optical phase-locked loops can exceed the speed of electrical phase-locked loops, but are complex [T. von Lerber 2009].

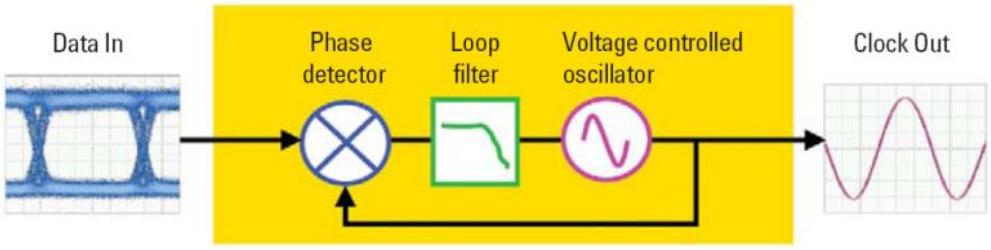

Figure 1.1: Schematic representation of a PLL in CR setup

The optical PLL speed is determined mainly by the photodiode and the phase comparator. Optical PLL can use nonlinear optical gates to measure the cross correlation of the data signal with the local oscillator. Response times of non-linear optical processes usually used in phase comparators are much shorter than those of electrical processes. These nonlinear gates can be made from gain modulated semiconductor optical amplifiers (SOAs) [S. Kawanishi 1988], amplitude modulated nonlinear optical loop mirrors [H. Bülow 1993], electro-absorption modulators [I. Phillips 1998], or LiNbO3 modulators [H. Dong 2004]. The cross correlation can also be realized by four wave mixing in an SOA [O. Kamatani 1994] or two photon absorption in a silicon avalanche photodiode

[R.Salem 2004]. These components could be used as O/E interfaces or/and as ultrahigh-speed phase comparators. Optical phase-lock loops may also be formed with oscillating electro-optic loops consisting of a Mach-Zehnder modulator and an amplifier [M. Chbat 1991] or an electro-absorption modulator with an amplifier [B.Mikkelsen 2000].

CR processes based on PLLs are well known for their high stability and high recovered clock quality characterized by sub picoseconds timing jitters. Beside these advantages, complexity is considered as the greatest drawback of the technique. Normally, the feedback loop increases the complexity and locking time of the system Moreover, PLL based CR functions require in general a long time for synchronization to the data stream. This last inconvenient make them not suitable for short optical packet traffic.

Filtering Method

Passive filtering seems to be the simplest technique for CR function in terms of physical principles. It can provide a simple and cost effective clock recovery solution. With passive filtering, the filter selects certain spectral components of the data signal to produce the clock signal. The optical filter could be an optical resonator exhibiting a Free Spectral Range (FSR) which is equal to the incoming signal rate. Possible filters include Bragg grating filters [J. Lee 2005], Fabry-Perot resonators and transversely coupled Fabry-Perot resonators [M. Jinno 1992], ring resonators [M. Jinno 1992], sideband filters [T. von Lerber 2007], and birefringent resonators [T. von Lerber 2006].

Fig.1.2 describes the operating principle of a clock extraction process using optical spectral line filtering technique. An optical data signal generated from a RZ intensity modulation consists of a continuous spectrum and discrete lines. The optical spectrum is centered on the optical carrier frequency f_0 and exhibits spectral lines at $f_0 \pm B$, where B denotes the transmitter clock frequency. All-optical CR is achieved by extracting the discrete lines at $f_0 \pm B$ and f_0. Result of the filtering process is an optical clock at the same wavelength as the incoming optical signal and at the same frequency as the transmitter clock.

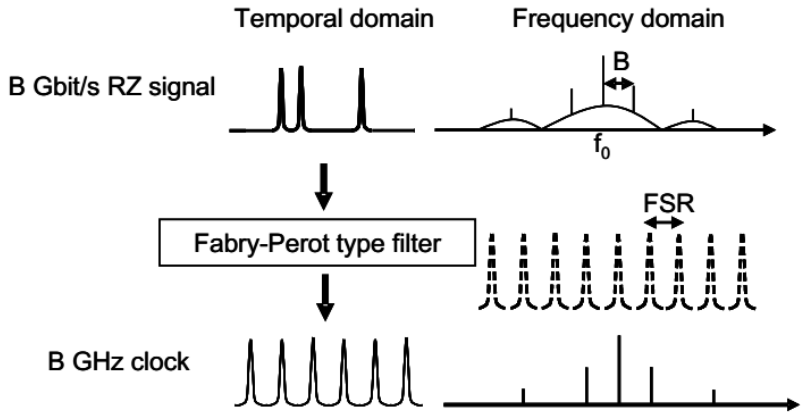

Figure 1.2: Operation principle of an Optical CR based on spectral line filtering technique

The three following conditions have to be satisfied: one of the filter resonance peaks superimposes on the optical carrier frequency, the optical filter FSR is equal to the transmitter clock rate and the optical carrier linewidth is narrower than the resonator bandwidth. The main limiting factor of the optical filtering technique is the requirement of high finesse filters. Besides, the technique suffers also from strong wavelength, polarization and sequence length dependences.

Injection locking of Self-Pulsating Lasers Method

Self-pulsating lasers offer clock recovery schemes that are simple and scalable to high data rates but have high manufacturing costs. With self-pulsating lasers, the data signal is optically injected to a laser, and the output is the recovered clock. The injected signal rate must be nearby the free pulsating frequency of the laser or a multiple of this frequency. A mode locked laser can be used with injection-locking in this manner [M.Jinno 1988] as can a two-section diode laser [M. Möhrle 1992], or a fiber based laser [K. Smith 1992]. From these techniques, passively mode-locked semiconductor lasers are significant as they typically exhibit lower phase noise and amplitude noise than self-pulsating lasers and less clock latency than fiber based devices.

The operation of the injection seeded optical clock is as follows: A passively mode locked laser produces optical pulses at its natural rate, which is proportional to the longitudinal mode spacing of the device cavity $c/(2L)$. Optical data bits from the

transmitter are injected into the mode-locked laser, where the data transmission rate is generally a harmonic of the clock rate. The injected optical bits serve as a seeding mechanism to allow the clock to build up pulses from the injected optical bits. As the injected optical bits and the internal clock pulse compete for gain, the continuous injection of optical bits forces the internal clock pulse to evolve and shift in time to produce pulses that are synchronized with the input data. The physical operating mechanism can also be understood by examining the operation in the frequency domain. From a frequency domain perspective, since the injected optical data bits are injected at a well-defined bit rate, the optical spectrum has a series of discrete line spectra centered around the laser emission wavelength and separated in frequency by the bit rate. Since the optical clock emits a periodic train of optical pulses, its optical spectrum is also a series of discrete line spectra separated by the clock repetition frequency. If the line spectra of the injected data bits fall within optical gain bandwidth of the optical clock, the injected line spectra will serve as seeding signals to force the optical clock to emit with line spectra similar to the injected signals. Since the injected data bits are repetitively pulsed, the discrete line spectra have the proper phase relation to force the clock to emit synchronously with the injected data.

1.4 Conclusion

In summary this chapter provides the background and motivation for the rest of the thesis. It discusses the need for All-Optical solutions and how clock recovery is the key functioning block to achieve high data rate in optical networks. Three techniques for optical clock recovery are classified according to their operational principle. Optical phase-locked loops can provide clock recovery at higher speeds than electrical clock recovery modules while self-pulsating lasers can provide a low cost method to recover the clock optically. All-optical clock recovery methods which use passive filtering can be advantageous if they can recover the clock signal from several WDM channels simultaneously. In 3R applications, the PLL technique is rarely used because of its complexity. On the other hand, the filtering technique and injection locking in oscillating systems could be exploited in both ‘Data driven’ and ‘Synchronous modulation’ 3R regenerators.

CHAPTER 2

Optical Phase Lock Loop Method

2.1 Introduction

Optical phase lock loops (OPLLs) are essentially the counterparts of PLLs in the optical domain, where a slave laser is used as the voltage controlled oscillator which tracks the frequency and phase of the optical signal of a master laser. The role of the phase detector is played by an optical component which in our case is semiconductor optical amplifier (SOA) for the rest of this chapter.

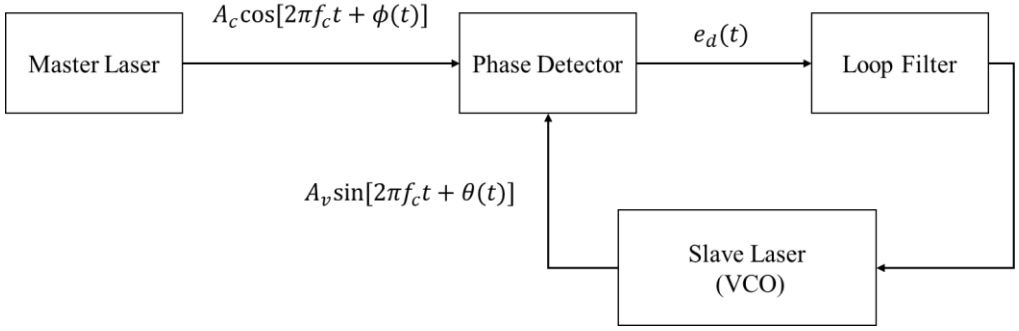

Figure 2.1: Typical Optical Phase Lock Loop

A technique for all optical timing extraction and clock recovery using OPLL is presented here. The technique is based on nonlinear all optical cross modulation inside semiconductor waveguides. In this technique, the all-optical timing extraction determines the timing difference between two counter-propagating optical pulses using the nonlinear SOA. The extracted timing information is used in conjunction with a balanced photo-detector to generate an electrical error signal. This error signal is used in a phase locked loop configuration to perform optical clock recovery.

2.2 Optical clock recovery using an SOA

In the following section we discuss in detail the optical clock recovery technique using semiconductor optical amplifier (SOA) as a nonlinear waveguide for all-optical timing extraction.

2.2.1 Pulse Propagation in SOA

In semiconductor waveguides, the gain and index of refraction depend on the carrier density, which is in turn affected by the injection current and optical intensity. The gain saturation equation, and the pulse propagation equation, describes the propagation of a signal through an SOA and the interaction of the signal with gain of the SOA. The expression for the gain in SOA is given by the Frantz-Nodvik equation [1].

$$G(t) = \frac{G_0}{G_0 - (G_0 - 1)\exp[-(P_{total}(t) +)/E_{sat}]}$$

This analytical equation is useful for modeling the gain variation during a short pulse, and was used in modeling our PLL model in Section 2.2.5 and laser system in Chapter 4.

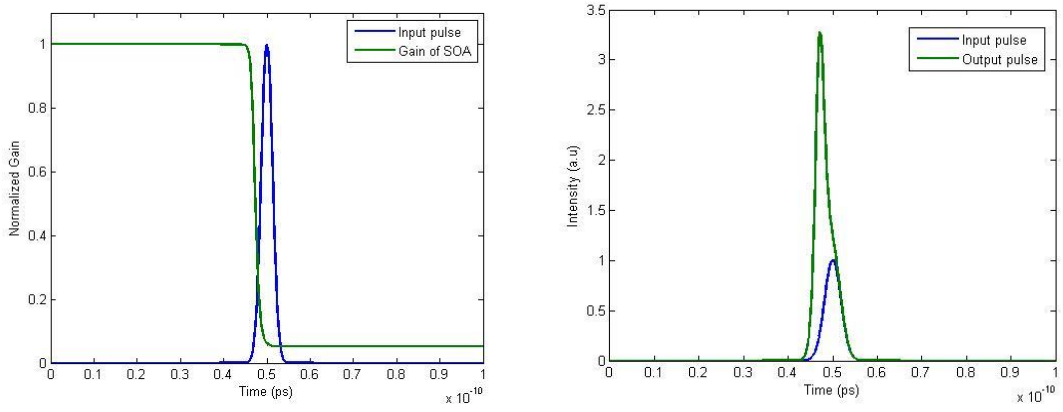

(a)

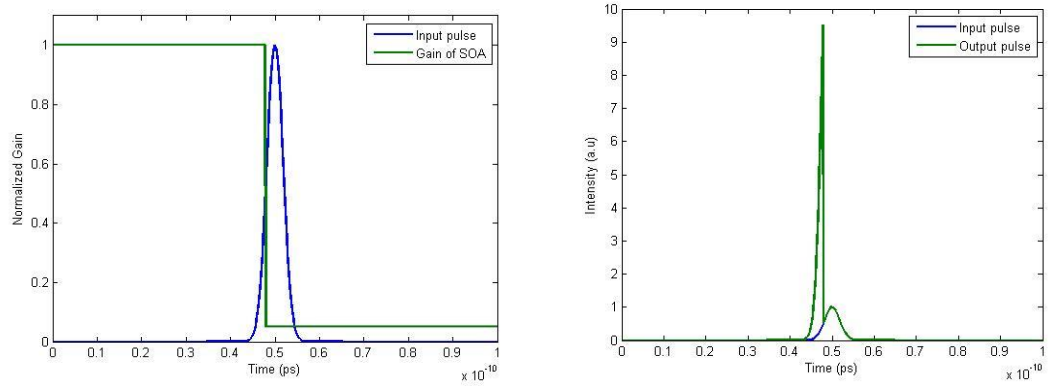

(b)

Figure 2.2: Time dependent gain of an SOA with 3ps FWHM input pulse (a) Real case (b) Ideal case for Gain=20.

In general, the peak power of picosecond pulses in nonlinear waveguides such as SOA causes saturation of gain through carrier excitation as shown in Fig.2.2a and the peak of the pulse is shifted at the output. The excitation and relaxation dynamics occur on a finite time scale that is determined by the material and structure of the waveguide. In ideal case we can consider that the gain saturates instantly just after the saturation energy is reached as shown in Fig.2.2b.

2.2.2 All-Optical Timing Extraction

Timing extraction is the process in which the arrival time of individual data bits is estimated and used subsequently to recover the phase and repetition rate of the optical clock. In this section we show how that can be achieved all-optically by using SOA nonlinear modulation.

Let us consider the case in which two counter-propagating pump pulses arrive at different times inside the nonlinear wave-guide. Both pulses contribute to the SOA transmission saturation. The leading pulse will saturate the gain, which in turn effects the transmission of the following arriving counter-propagating pulse. Therefore, a pulse sees a low transmission if it is preceded directly by a sufficient intense counter-propagating pulse that allows pre-saturation to the medium gain. Given that the nonlinear device has two possible outputs, one for each counter-propagating pulse steam, as shown in Fig.2.3a, is simulated to give a delay-dependent peak power transmission for each output as shown in Fig.2.3c for ideal case of SOA where gain saturates instantly and does not recover.

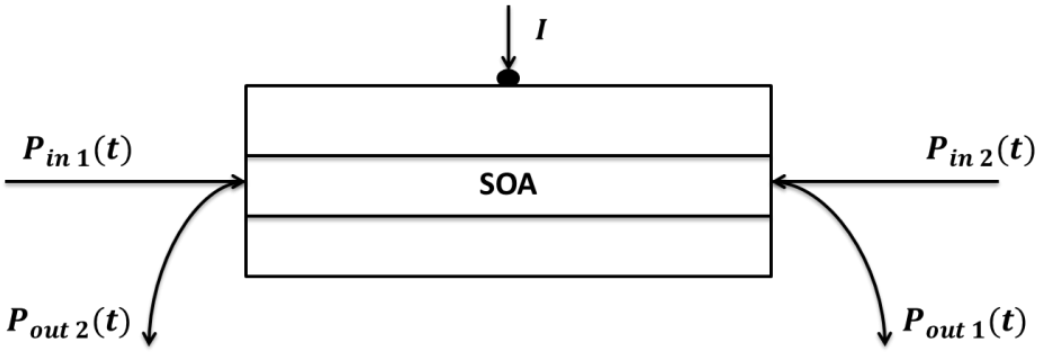

Figure 2.3: (a) Schematic configuration of all-optical timing extraction

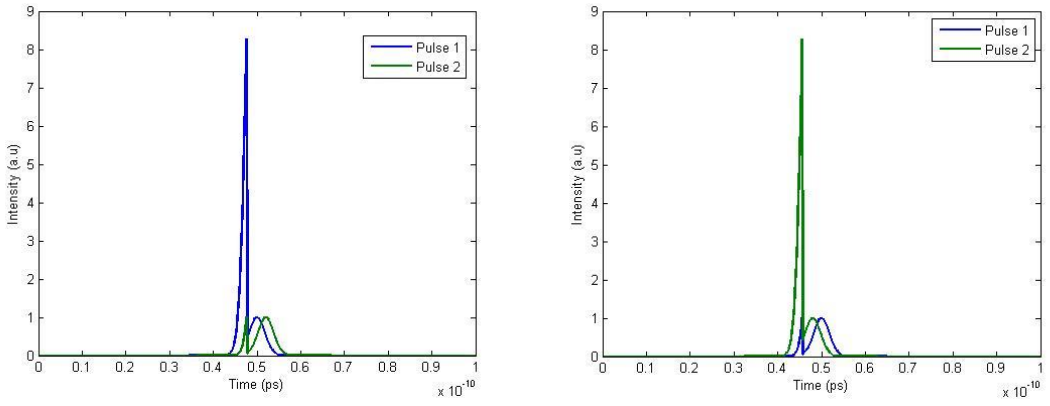

Figure 2.3(b) Idealistic SOA output pulses for delay of +2 ps and -2 ps

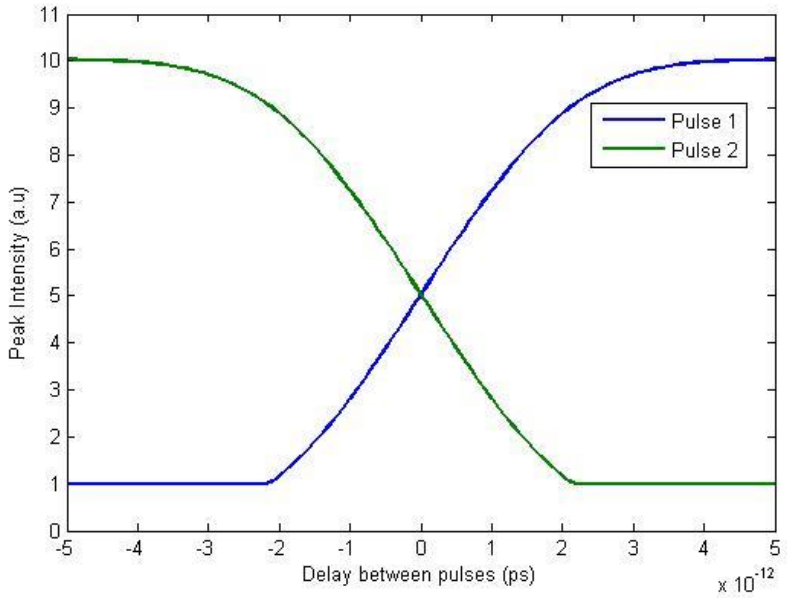

(c)

Figure 2.3: (c) The Ideal SOA simulated transmitted peak power from each output as a function of timing delay between the two pulses inside the wave-guide.

Fig.2.3c illustrates the transmitted peak power versus the relative arrival time delay between the two counter-propagating pulses. Each of the two curves represents one output from each side of the idealistic case of SOA. Zero delay corresponds to the moment at which the two pulses arrive simultaneously inside the wave-guide. Therefore, these two curves provide timing information about the two counter-propagating pulse streams.

Based on this principle, two optical beams with the same or different wavelengths or polarizations are launched simultaneously into a realistic case of SOA in a counter-propagating configuration. Each of the two counter-propagating streams can be considered as a pump and a probe at the same time. The first beam (referred to as data) is a pulse train encoded with binary digital information using amplitude shift keying. The second beam (referred to as clock) is a stable pulse train produced by an optical pulse source with a repetition frequency close to that of the data and has a relatively low timing jitter. The amount of transmission change, however, depends on the relative delay between the data and clock signals inside the device. Therefore, the transmitted power of the data and clock signal depends critically on the relative arrival timing of the two pulses inside the wave-guide.

2.2.3 Error signal generation

In principle, the error signal provides complete information on the timing error between the data and clock pulses. This timing error can be compensated by proper tuning of the repetition frequency and phase of the optical pulse source. Here, we generate the error signal by using a balanced photo-detector as shown in Fig.2.4a. The SOA has two outputs; each goes to one of the detector inputs. The balanced photodetector takes the difference between its two detected electrical signals and produces an electrical error signal at its output. The output is zero if the two inputs are identical. Fig.2.4b shows a typical error signal. The fundamental frequency of the error signal (10 KHz) equals to Δf and one full period of the error signal corresponds to a drift of 100 ps between the data and clock pulses. The polarity of the generated error signal indicates which pulse stream is ahead of the other, while the amplitude of the error signal indicates the amount of the delay between the two pulse streams. The fast slope represents the interval during which the two pulses arrive almost simultaneously inside the nonlinear waveguide, while the slow slope represents the arrival of the two pulses far apart.

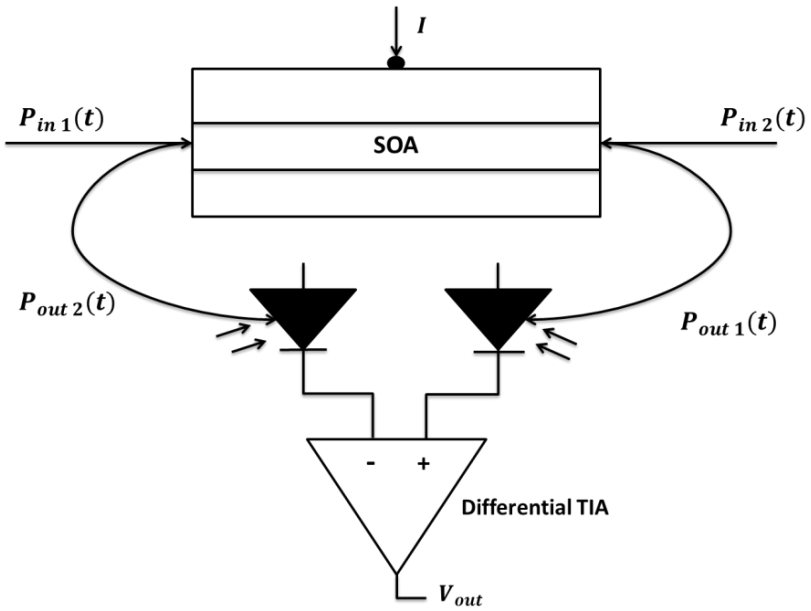

Figure 2.4: (a) Schematic for error signal generation

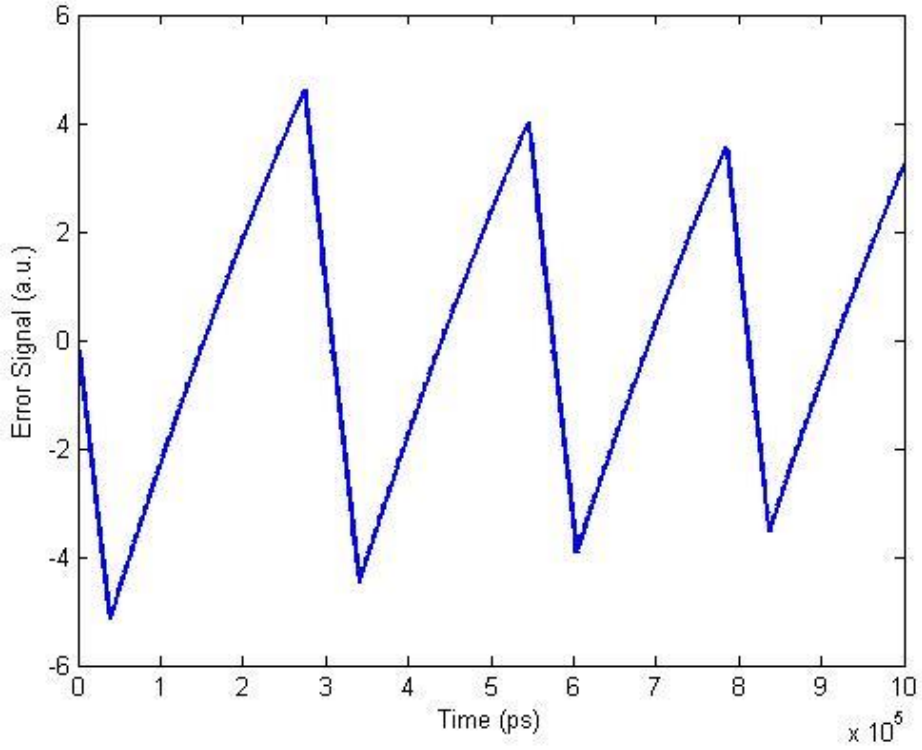

Figure 2.4: (c) Simulated error signal versus time with an open loop feedback. The frequency difference between the data and clock is 10 kHz, LPF Bandwidth ≅ 15 kHz

2.2.4 Optical Clock Recovery System

The all-optical timing extraction technique using counter-propagation pulses gives information about the amount of delay between the two pulses and which of the two pulses arrives first. This kind of information is important for optical clock recovery. Assuming that one of the two counter-propagating pulse streams is the data while the other is the clock, the all-optical timing extraction can be used to generate a timing error signal that in turn can be used to perform optical clock recovery.

Fig.2.5 shows a typical configuration for the optical clock recovery system. The clock signal was derived from an optical pulse source, such as a semiconductor mode locked diode laser (MLL), produces a stable optical pulse train. The data signal is an RZ bit stream that counter-propagates with respect to the clock signal inside the nonlinear wave-guide SOA. The transmitted clock and data through the device are then split off and detected by a balanced photo-detector to produce the electrical error signal. This error signal is fed back to the VCO input to adjust its repetition rate. The VCO in turn drives the optical pulse source to adjust its repetition frequency. The repetition rate and phase of the optical pulse source stabilizes only when the clock and the data are synchronized.
In general, this system can recover a sub-harmonic clock from the incoming data with an optical clock source running at the data base-rate.

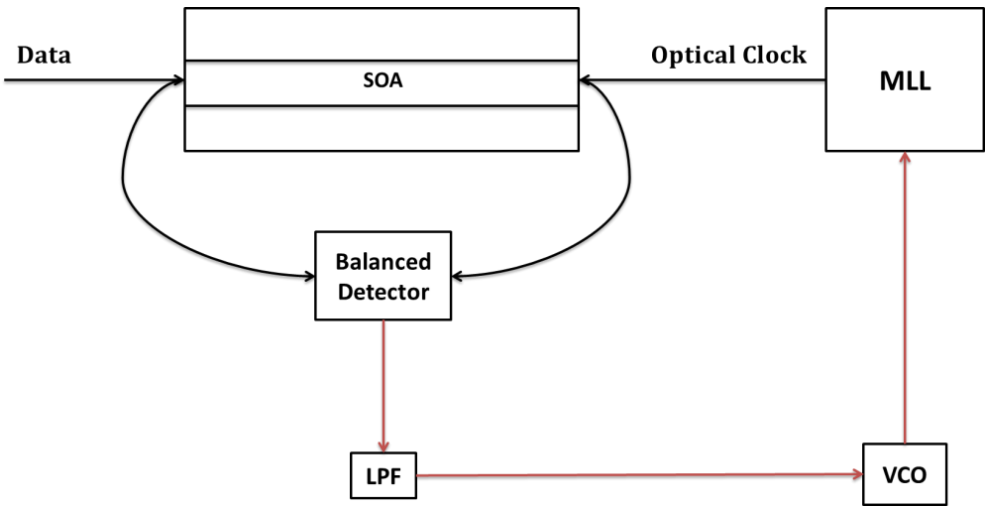

Figure 2.5: Simulation setup for optical clock recovery system

2.2.5 Numerical Model

In this section we present a model for optical clock recovery system using SOA. The model is based on nonlinear optical pulse propagation inside gain medium [1]. The basic equations that govern the pulse propagation and saturation analysis in SOA are:
Propagation along '+ z' direction:

$$\left(\frac{\partial}{\partial x}+\frac{n}{c}\frac{\partial}{\partial t}\right)P_1(z,t)=g(z,t)P_1(z,t) \tag{2.1}$$

Propagation along '$-$z' direction:

$$\left(\frac{-\partial}{\partial x}+\frac{n}{c}\frac{\partial}{\partial t}\right)P_2(z,t)=g(z,t)P_2(z,t) \tag{2.2}$$

Gain saturation and relaxation:

$$\frac{\partial}{\partial t}g(z,t)=\frac{g_0-g(z,t)}{\tau_r}-\frac{g(z,t)P_{total}}{E_{sat}} \tag{2.3}$$

Where 'n' is the medium refractive index, 'c' is the speed of light in vacuum, $P(z,t)$ is the optical power at point 'z' and time 't', $g(z,t)$ is the gain coefficient, 'τ_r' is the recovery time, and '$Esat$' is the saturation energy for the gain medium.

The above three equations are difficult to solve analytically; therefore, we solved them numerically and solved in MATLAB. We assumed the SOA is divided into 'N' sections along the device length, as shown in Fig.2.6, to model the gain spatial effect on propagating pulses along the device. The output of each section becomes the input to the following section. For a single section with a small length 'Δz', with a small error, the two counter propagating pulses can be considered to be co-propagating.

For each time step in numerical simulation, we can find the saturated gain of each segment using same procedures as [2]. The output power $P_{out\,1}(t)$ can be written as a function of input power $P_{in\,1}(t)$:

$$P_{out\,1}(t)=G(t)*P_{in\,1}(t) \tag{2.4}$$

Similarly,

$$P_{out\,2}(t)=G(t)*P_{in\,2}(t) \tag{2.5}$$

where $G(t) = \exp\big(g(t)\big)$ is the time varying partially saturated gain:

$$G(t) = \frac{G_0}{G_0 - (G_0 - 1)\exp[-\big(P_{in\,1}(t) + P_{in\,2}(t)\big)/E_{sat}]} \tag{2.6}$$

Equation.2.6 expresses the gain saturation with time as a function of total input power $\big(P_{total}(t) = P_{in\,1}(t) + P_{in\,2}(t)\big)$. This equation does not take into account the gain recovery time. However, at each time step, the saturated gain recovers to its initial value 'Go' with a recovery time 'τ_r' according to equation.

$$\frac{\partial}{\partial t} g(z,t) = \frac{g_0 - g(z,t)}{\tau_r} \tag{2.7}$$

We find out that three sections are enough for a good approximation. Fig.2.6 shows a schematic configuration of the PLL open feedback loop

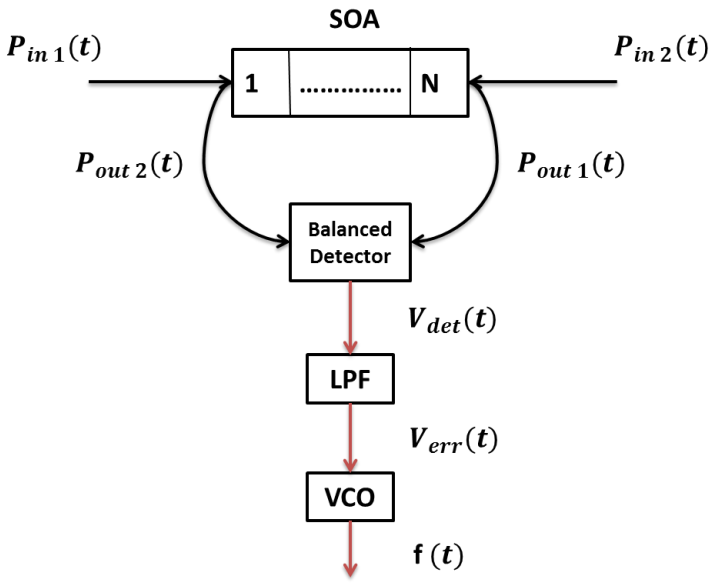

Figure 2.6: Schematic configuration of PLL open loop feedback

Using eq. (2.4) & (2.5), the balanced photo-detector output voltage can be expressed as:

$$V_{det}(t) = f(\varphi) = [P_{out\,1}(t) - P_{out\,2}(t)]\frac{\eta e}{\hbar w} Z_L \tag{2.8}$$

Where 'η' is the photo-detector quantum efficiency, 'e' is the electron charge, '$\hbar$ ' is Planck's constant, 'w' is the optical frequency in radian/sec., 'Z_L' is the photo-detector load impedance. The balanced photo-detector output voltage $V_{det}\,(t)$ is a function of the

time delay between the two input counter-propagating pulses, or the phase difference 'φ' between the RF of signal and clock. The $f(\varphi)$ can be found by numerically solving for $P_{in\,1}(t)$ and $P_{in\,2}\,(t)$ as described above.

The signal from the balanced photo-detector goes through a low pass filter (LPF). The output of LPF is the error signal $[V_{err}(t)]$ which is obtained by solving:

$$\frac{dV_{err}(t)}{dt} = V_{det}\,(t) - \frac{V_{err}(t)}{\tau_f} \tag{2.9}$$

Where 'τ_f' is the LPF time constant. This error signal is multiplied by the feedback gain factor, and then used to control the repetition frequency of the optical clock pulses, which is controlled by the VCO.

The VCO instantaneous repetition frequency $\nu(t)$ is given by

$$2\pi.\,\nu(t) = \frac{d\varphi}{dt} = K_1.V_{err}(t) \tag{2.10}$$

Where

$$K_1 = 2\pi.G_eK_{VCO}$$

$$\Delta\varphi = 2\pi\Delta t/T$$

G_e is the feedback voltage gain. 'K_{VCO}' is the VCO coefficient (Hz/V), and 'T' is the pulses repetition period. The holding range of the PLL can be estimated from the error signal. The edge of the holding range is reached at the point where the slope of the error signal changes [3].

2.2.6 Simulation Results

Fig.2.7 shows the simulated transient response of the error signal amplitude and the delay Δt between the clock and data versus time using the SOA at unsaturated gain coefficient $= 2$ for different input data rates. The frequency offset between the data and clock repetition rates is set to 1MHz. The clock recovery system was tested at different bit rates, to check the performance. It was tested at 160, 80, 40, 20, and 10 Gbit/s and then the timing jitter was calculated.

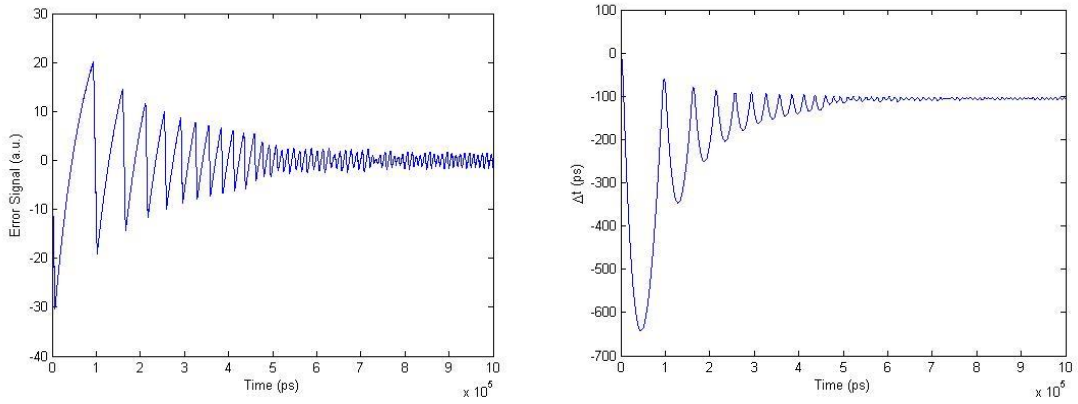

(a)

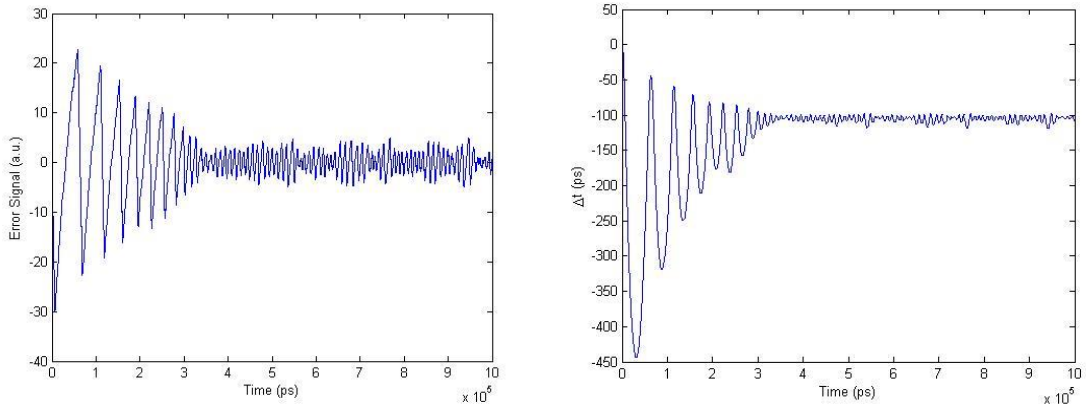

(b)

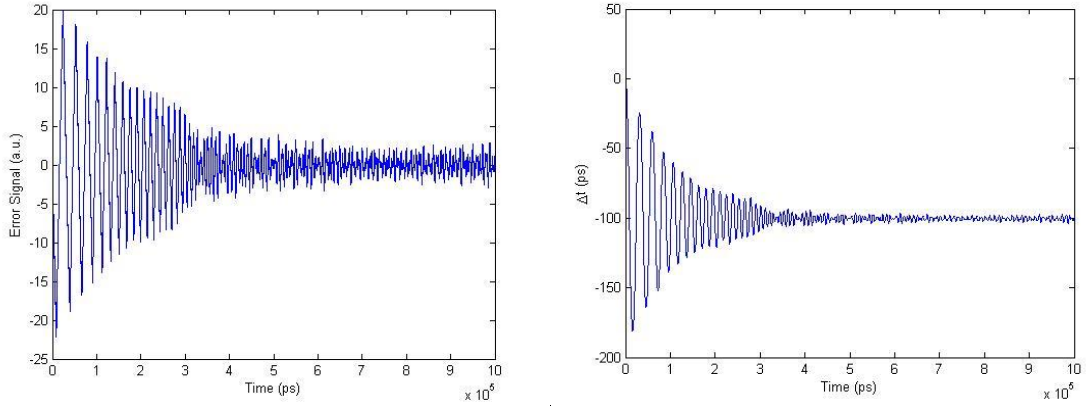

(c)

Figure 2.7: The simulated transient response of the error signal using SOA with a $2^7 - 1$ PRBS data, running at (a)10Gbit/s (b)40Gbit/s (c)160Gbit/s, LPF BW≈100MHz,$\Delta f =$ 1MHz

Similar results were obtained for the case of nonlinear semiconductor waveguide Electro Absorption Modulator (EAM) as shown in Fig.2.8 where the loss saturates (absorption saturation) when a peak pulse is incident. The magnitude of the error signal in case of SOA is larger because of its gain.

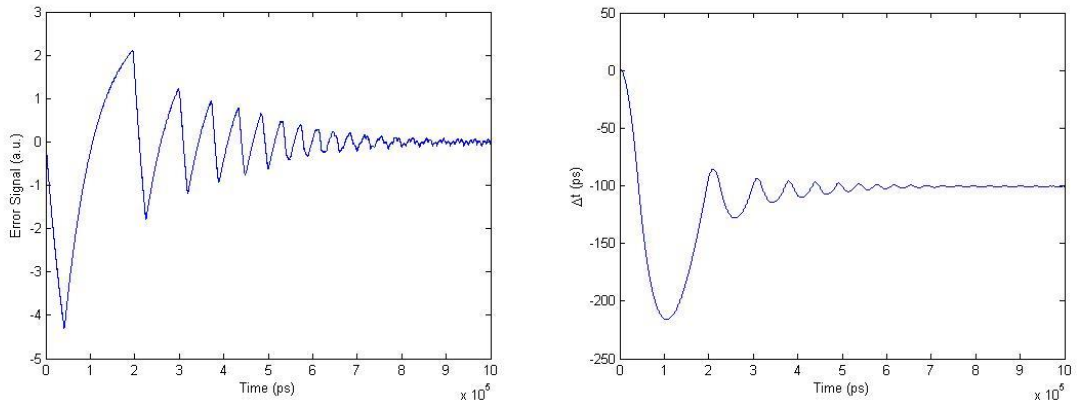

Figure 2.8: The simulated transient response of the error signal using EAM with a $2^7 - 1$ PRBS data, running at 160Gbit/s, LPF BW≈100MHz, $\Delta f = 1$MHz

The simulation results show a successful lock operation up to 160 Gbit/s using SOA and EAM. The system shows a good locking in each case. From the model, we observed that the timing jitter is related to the error signal slope 'S' which is defined as

$$S = \frac{dV_{err}(t)}{d(\Delta t)} \tag{2.11}$$

where Δt is the time of the error signal slope, and '$V_{err}(t)$' is the error signal voltage. The slope of the error signal can be measured from the error signal when the clock is unlocked, as shown in Fig.2.4b. As discussed earlier, one full period of the error signal corresponds to a drift equal to one repetition time period between the data and clock pulses (e.g. 100ps). Therefore, the error signal time is proportional to the time delay between the data and clock pulses. Over large interval the slope is approximately constant, and it can be calculated from the data.

After locking, the same calculated slope can be used to estimate the timing jitter between the data and clock. In that case, 'Δt' corresponds to the timing jitter between the data and clock pulses, and '$V_{err}(t)$' is the fluctuation of the error signal amplitude after locking,

which is proportional to the system noise. Therefore, the timing jitter is expected to increase with higher bit rates as the data input peak power. The model has been used to calculate the timing jitter in the SOA case at different bit rates. Fig.2.9 shows the r.m.s timing jitter in (fs) at different data bit rates up to 160 Gbit/s.

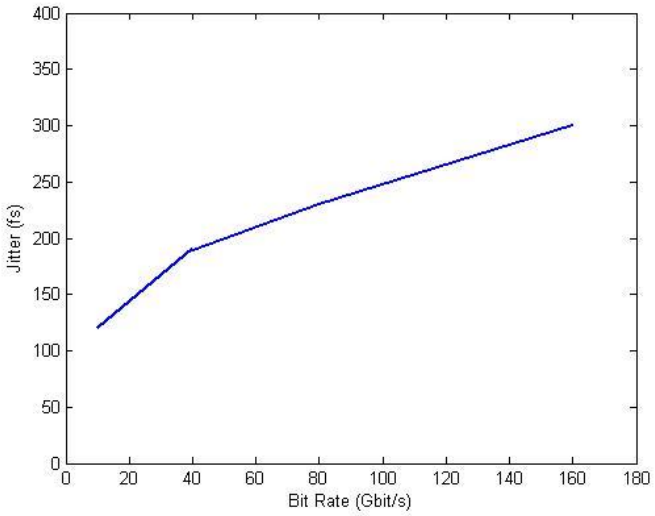

Figure 2.9: The simulated timing jitter as function of different data bit rates.

In case of 10 Gbit/s input data, we obtain the lowest r.m.s timing jitter, which is ≤ 120 fs. Assuming a fixed input peak power at all data rates in the model, the jitter should stay approximately constant.

2.3 Conclusion

In this chapter the technique for all optical timing extraction and clock recovery is presented. The all-optical timing extraction determines the timing difference between two counter-propagating optical pulses using the nonlinear optical wave-guides. The extracted timing information is used in conjunction with a balanced photo-detector to generate an electrical error signal. This error signal is used in a phase locked loop configuration to perform optical clock recovery.

Simulation results show the transient response and locking behavior of the clock recovery system at different data rates up to 160 Gbit/s with minimum jitter. In general, this system can recover a sub-harmonic clock from the incoming data with an optical clock source running at the data base-rate.

CHAPTER 3

Filtering Method

3.1 Introduction

Optical phase-locked loops can provide clock recovery at higher speeds than electrical clock recovery modules while self-pulsating lasers can provide a low cost method to recover the clock optically. All-optical clock recovery methods which use passive filtering can be advantageous if they can recover the clock signal from several WDM channels simultaneously. An effective method of using a Fabry-Perot Filter (FPF) as optical tank followed by a semiconductor optical amplifier (SOA) as amplitude equalizer was demonstrated to recover optical clocks from incoming return-to-zero (RZ) data signals at 10 Gb/s and 40 Gb/s. Compared with other clock recovery methods, this scheme features with extremely structural simplicity, low cost of components and the potential of being integrated.

In this chapter we discuss all-optical clock recovery based on a Fabry-Perot Resonator or optical tank circuit. I demonstrate all-optical clock recovery from optical signal with RZ on-off-keying (RZ-OOK) modulation format by using a FPF as an optical tank, followed by a SOA and a filter as an amplitude equalizer. We studied in detail the setup composed of a high-finesse FPF and an SOA in an optical communication system, and particularly the sensitivity to the pattern sequence length of each configuration: the filter alone, and then the combination of the filter and the SOA. We use Bit Error Rate assessment and Eye opening factor to demonstrate its system compatibility and to evaluate both its pattern sequence length tolerance and its clock locking range.

3.2 Optical Resonators

Optical resonators, including Fabry-Perot resonators, are devices that allow light to circulate in a closed path. Optical resonators are also considered optical cavities which store light for a period of time. A Fabry-Perot resonator consists of two parallel reflective

surfaces. These two surfaces may consist of partially reflective mirrors or the interface between two materials with different indices of refraction. As illustrated in Fig.3.1, a pulse enters one end of the resonator. After propagating through the resonator, part of the pulse is transmitted through the second surface and the remaining energy is reflected back towards the first surface. Part of this remaining energy reflects off the first surface and the process repeats itself. If a single pulse is input into the resonator, a series of pulses with exponentially decaying amplitudes will be output. The temporal separation of the pulses corresponds to the roundtrip time of the cavity.

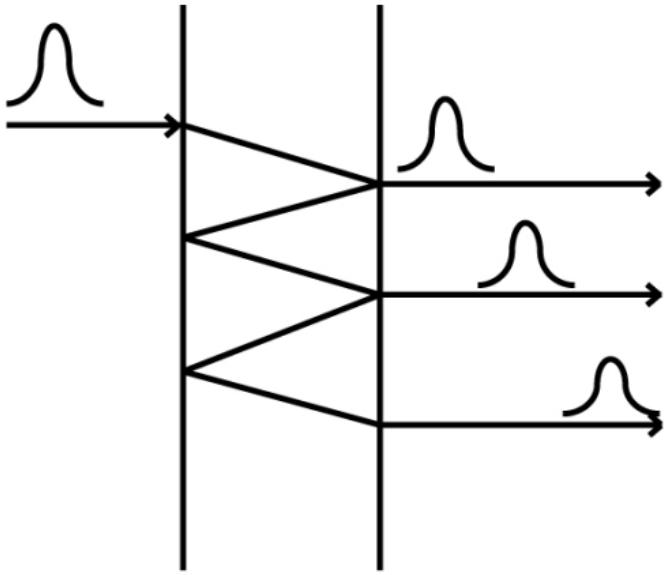

Figure 3.1: Illustration of pulse propagation in Fabry-Perot Resonator

The Fabry-Perot resonator has unique spectral properties which lends itself to clock recovery. The transmission function of the Fabry–Perot resonator is given by:

$$T = \frac{(1-R)^2}{(1-R)^2 + 4Rsin^2\left(\frac{\phi}{2}\right)} \tag{3.1}$$

where $\phi = 4\pi nl/\lambda$ is the round-trip phase shift, R is the reflectivity of each surface, n is the index of refraction of the resonator, l is the resonator length, and λ is the free-space wavelength of light. Equation (3.1) is periodic in terms of round-trip phase shift which in turn is a function of wavelength as shown in Fig.3.2a. The Fabry-Perot resonator will

transmit certain wavelengths of light while filtering out others. The spectral period of (3.1) is the free spectral range and is:

$$FSR = \frac{c}{2nl} \tag{3.2}$$

where c is the speed of light in vacuum. The Fabry-Perot resonator presents a transmission maximum every free spectral range. The bandwidth of the transmission maximum is:

$$\delta v = \frac{c}{2nl}\frac{1-R}{\pi\sqrt{R}} \tag{3.3}$$

And the cavity finesse is given by:

$$F = \frac{FSR}{\delta v} = \frac{\pi\sqrt{R}}{1-R} \tag{3.4}$$

The cavity Finesse increases when the reflectivity of the mirrors is increased as shown in Fig 3.3. The resonator photon lifetime is:

$$\tau_p = \frac{1}{2\pi\delta v} \tag{3.5}$$

These parameters are used to characterize Fabry-Perot resonators.

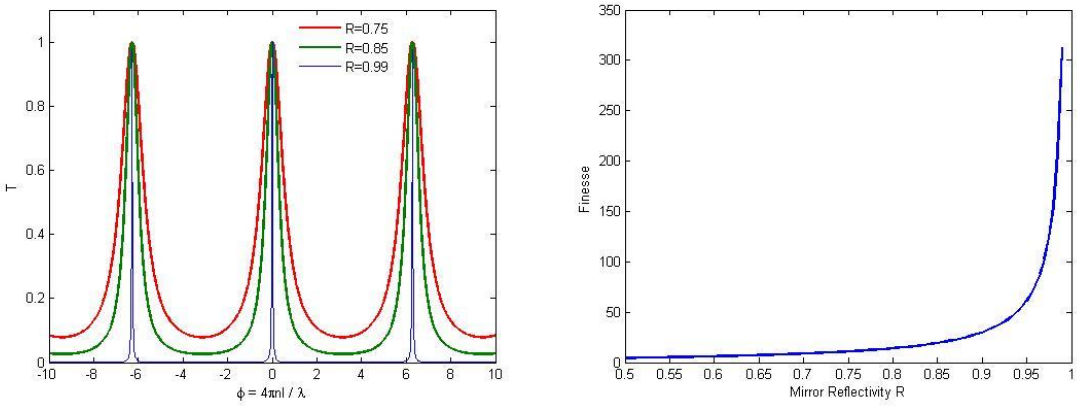

Figure 3.2: (a) The Transmitted Intensity (b) Reflectivity Finesse versus Mirror Reflectivity R of a Fabry-Perot Resonator

3.3 Optical Clock recovery using Fabry-Perot Filter

In this work I consider clock recovery using an optical tank circuit. An optical tank circuit consisting of a Fabry-Perot Filter is used as clock recovery device. The filter is tuned such that its free spectral range (FSR) corresponds to clock tone frequency of data

as shown in Fig.1.2 from Chapter 1. The carrier frequency and clock tones are filtered by the tank circuit, and the resulting heterodyned output is the clock signal.

3.3.1 Simulation Setup

The optical clock recovery (OCR) scheme used is shown in Fig.3.3. It consists of a FPF whose Free Spectral Range (FSR) is equal to the residual line frequency separation of the 10 GHz RZ input data spectrum. The clock recovery technique is a narrowband filtering of the signal modulation lines. The SOA operating in saturation regime is then used as a power equalizer for reducing the residual amplitude clock modulations due to light polarization effects or mismatching between the FSR and the line spacing in the optical spectrum.

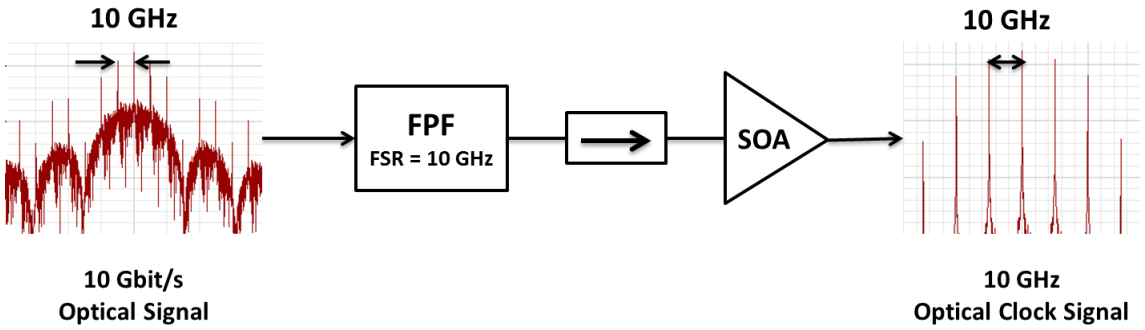

Figure 3.3: All-Optical clock recovery setup using Filtering Method

In order to specify the characteristic of the optical clock recovery system, we carried out a numerical simulation of the filtering process, using Optisystem commercial software. For this simulation we used a pattern sequence length from 2^7 to 2^{11} (127 to 2048 bits per sequence) and RZ data signal at 10Gbit/s with Gaussian pulse distribution. I was unable to simulate longer sequences because of the limitations of my computational equipment. The physical parameters used for the simulation are: the SOA input power equal to 2.4dBm, the SOA current drive equal to 300 mA, the SOA length equal to 500 μm, the effective area equal to 2.4×10^{-13} m^2, and the confinement factor equal to 0.3.

The Rx is composed of an erbium-doped fiber amplifier (EDFA) and an optical bandpass filter (bandwidth 125 GHz) in order to keep a constant input power of 0dBm at the photodetector input, and then, to be able to characterize the Rx sensitivity. The optoelectronic Rx is optically preamplified and composed of an optical attenuator, an

optical amplifier, a bandpass optical filter, the photodetector, and the electronic processing circuits. It is then possible, by reducing the input signal power, to reach the Rx threshold sensitivity and plot the BER versus the input optical power. This characterization is a quantitative analysis usually used in transmission experiments. Using these two qualitative and quantitative approaches, varying the filter finesse we observed the characteristic degradation of the clock quality due to long sequence of spaces. This degradation is evaluated using a technique based on the re-modulation of the recovered clock driven by the electrical data from the transmitter which gives bit error rate (BER) analysis in a data transmission environment at 10Gbit/s, which gives a quantitative estimation of clock quality.

3.3.2 Remodulation Technique

The remodulation technique is used to estimate the compatibility of the optically recovered clock (RCK) with optical transmission system requirements. BER measurements are an appropriate quantitative criterion of the degradation introduced by the OCR as compared to a reference without a clock recovery operation. The remodulation technique is based on the remodulation of the RCK by the electrical data in order to produce an optical data signal (RCK-Data). BER measurements are then carried out on this signal. Fig.3.4 depicts the setup of the remodulation technique used.

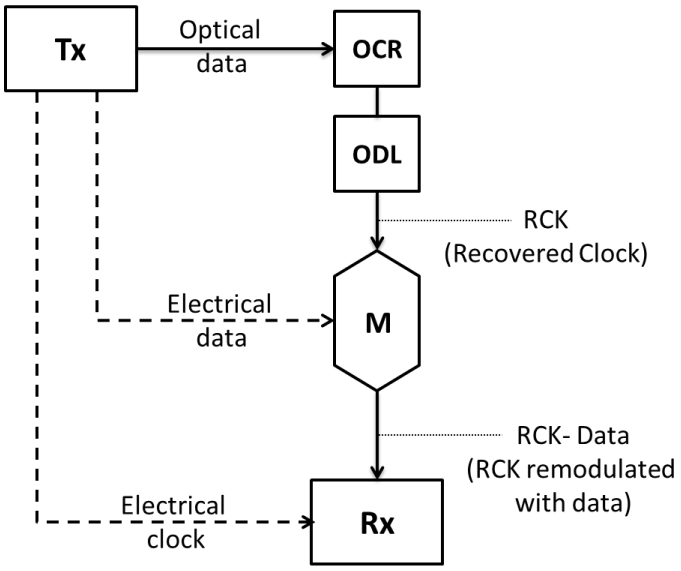

Figure 3.4: Setup of the remodulation technique used to study RCK quality.

The transmitter (Tx) generates an RZ optical data signal. The BER reference is obtained by directly connecting the Tx and the receiver (Rx) (back-to-back configuration). In the next step, the optical data signal is then injected into the OCR device under test. The recovered optical clock is delayed in the optical delay line (ODL) in order to keep it in phase with the electrical data in the optical modulator (M), where it is remodulated to become the RCK-Data signal. RCK-Data signal is then analyzed with the error detector of the Rx block. Any noise affecting the RCK is directly transferred onto the remodulated signal and can cause errors, which provide a quantitative estimation of the RCK quality. Since we use the same direct electrical clock for Rx synchronization in both cases, any degradation of the BER can be attributed to noise on the RCK. In the following study, we use this remodulation technique extensively in order to investigate the influence of the PRBS length on the OCR process.

Eye Opening Factor

Eye Opening Factor (EOF) is used to compare the quality of the re modulated clock to the input data signal from the transmitter. By this way it is possible to evaluate the degradation introduced through the filter and also the enhancement brought through the SOA. This technique has been recently proposed for experimental characterization of optically recovered clocks. The EOF definition is given by the following expression:

$$\mathrm{EOF} = \frac{(\mu_1 - \sigma_1) - (\mu_0 - \sigma_0)}{(\mu_1 - \mu_0)} \tag{3.6}$$

The EOF is deduced from the eye diagram and calculated after the remodulation step. The variables μ_0 and μ_1 are the mean values conditional to marks and spaces, respectively, and σ_0 and σ_1 are the associated rms values. In the simulation software, the EOF is directly measured using the statistical data from the eye diagram construction.

EOF is measured on the re-modulated clock, firstly after the FPF, and then after the SOA, to compare them to the transmitted signal. The Eye Opening factor value of the input signal (without degradation) is 1 and corresponds to an extinction ratio of more than 15dB.

3.3.3 Simulation Results

To begin with, we focus my study on the intrinsic sensitivity of the passive filtering of the FPF without SOA. Then we focused on the sensitivity of the tandem, which is composed of the FPF followed by the SOA.

Fig.3.5 depicts the simulated evolution of the EOF versus the finesse value for the FPF alone. It shows that EOF is improved when we increase the finesse of the filter but reduces when the bits per sequence is increased. The number of bits per sequence was varied from $2^7 - 1\ to\ 2^{11} - 1$ (i.e., 127–2048 bits/sequence) at a bit rate of 10 Gbit/s. The insets in Fig.3.5 present the eye diagram of the re-modulated clock for each configuration, for a FPF finesse value of 500.

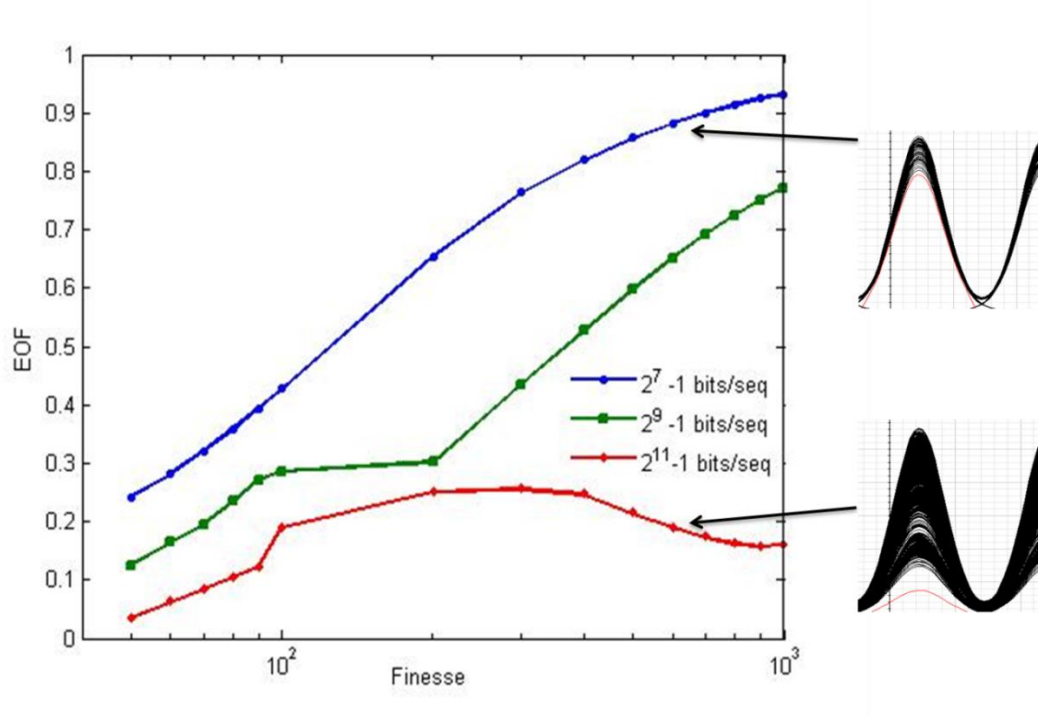

Figure 3.5: EOF Vs Finesse for the FPF alone case

It shows that the Eye Opening factor estimated on the re-modulated recovered clock is enhanced when increasing the FPF finesse and tends towards 1 for lower bit sequence length. We were unable to simulate longer sequences because of the limitations of my computational equipment.

Fig.3.6 shows that the EOF is improved when the SOA is used in tandem. The insets in the figure represent the eye diagram of the re-modulated clock for each configuration, for

a FPF finesse value of 100. With this simulation result we show clearly that FPF output clock quality is enhanced through the SOA by reducing amplitude fluctuations.

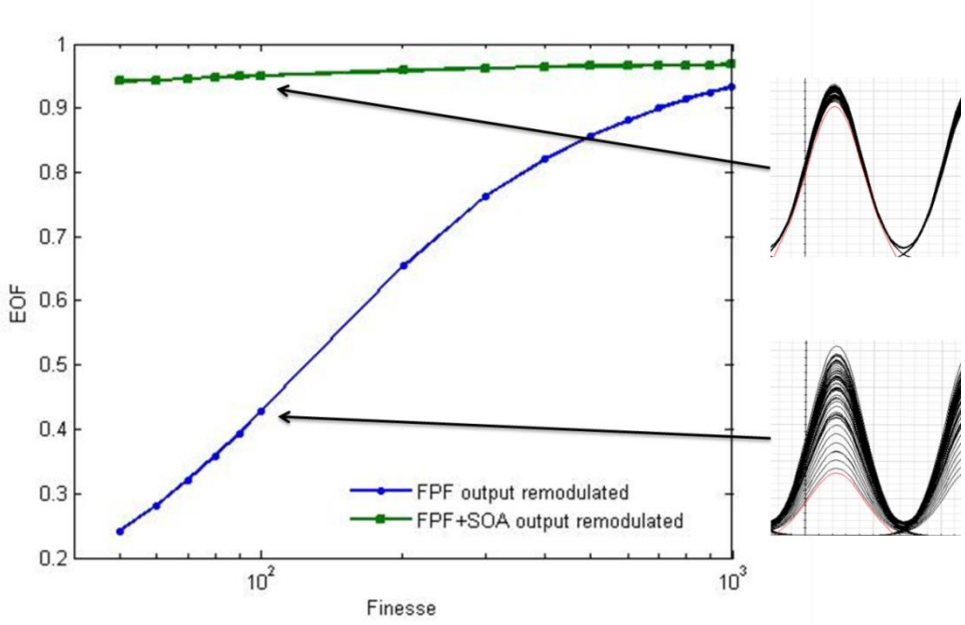

Figure 3.6: Eye opening factor Vs Fabry-Perot Filter finesse for $2^7 - 1$ bits/seq

Fig.3.7 shows the EOF of the remodulated recovered clock with SOA in tandem with FPF for various bit sequence lengths. From this plot we can say that even the SOA is sensitive to pattern effects as widely reported in literature.

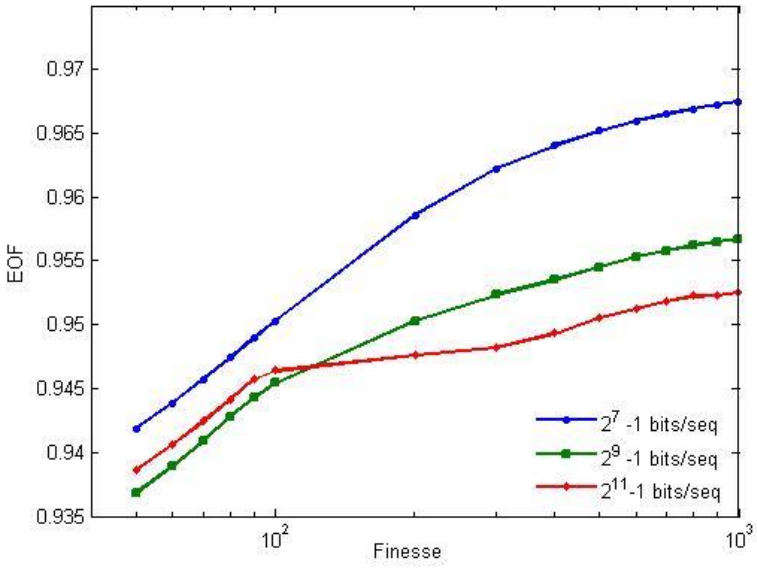

Figure 3.7: EOF vs Finesse for FPF + SOA output remodulated

Fig.3.8 shows that the EOF is improved when the SOA is present, for all sequence lengths, thus demonstrating the global efficiency of the SOA in this clock recovery configuration. This result shows that only short sequences of data (n = 7) are compatible with this OCR configuration.

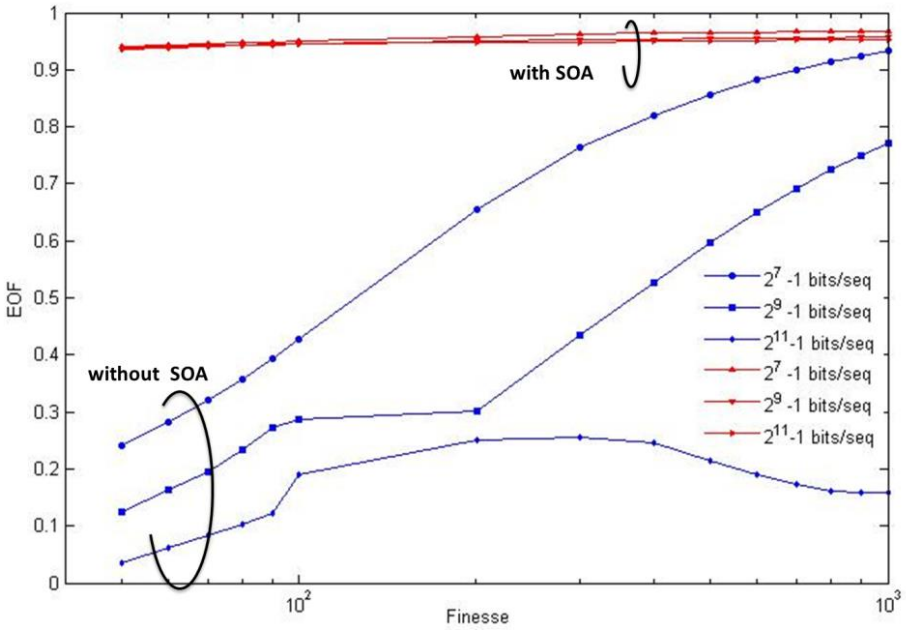

Figure 3.8: EOF vs Finesse

3.4 Conclusion

In summary, we presented in this section, a numerical simulation in order to highlight the effect of the OCR sensitivity to the number of zeros in the data sequence. We show that the SOA after the FPF enhances the RCK quality as compared to the configuration without SOA. We also show that this behavior depends on the sequence length and the finesse value. This study gives information on the eye diagram opening as a preliminary step in a clock recovery system characterization.

CHAPTER 4

Injection Locking Method

4.1 CW Injection Locking Theory

CW injection locking is a method of controlling the optical frequency of a CW laser. The technique entails injecting a relatively weak oscillator signal of optical frequency ω_1 from an external source into a laser, which on its own produces a strong oscillating signal at optical frequency ω_0 . Under certain conditions, the laser will produce an oscillating signal at ω_1, and the phase of this output can be theoretically predicted. In this case, the laser is said to be injection locked by the weaker external CW signal. The theory of CW injection locking is well understood [1], and a brief review of the basic concepts is presented here.

To begin, consider a linear laser cavity with gain and loss factors δ_m and δ_c, respectively, and field reflection and transmission coefficients ρ and τ, respectively, at the cavity facets. Suppose this laser produces a single mode CW output with optical frequency ω_0. In the absence of injection, this CW output is called the free running output of the laser. Now, suppose an external CW signal with optical frequency ω_1 is injected into one facet of the laser, as depicted in Fig.4.1. Let $\tilde{E}_{circ}$ be the phasor representation of the total optical wave traveling around the cavity, measured at a plane just inside the input facet and traveling into the laser. Then, $\tilde{E}_{circ}$ is the sum of two different sources of optical waves. Let $\tilde{E}_{refl}$ be the portion of the circulating wave which comes from the optical signal inside the laser cavity reflecting off the input facet. Let $\tilde{E}_{inj}$ be the portion of the circulating wave which comes from the injected signal. The signal $\tilde{E}_{inj}$ is, in turn, the portion of the external incident wave $\tilde{E}_{inc}$ which is transmitted through the input facet of the laser. A portion of $\tilde{E}_{inc}$ is also reflected from the input facet. The importance of this portion will be discussed in the section 4.2**.**

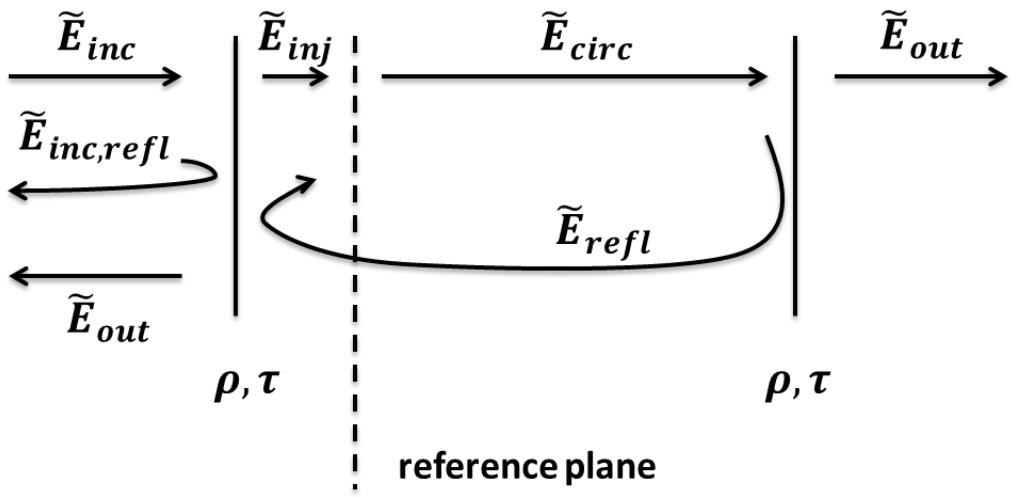

Figure 4.1: Schematic model for Injection Locking

For self-consistency, the reflected wave must be equal to the circulating wave that left the reference plane one round trip time *TRT* earlier, after it has experienced the gain, loss, and phase shift associated with the laser cavity. This self-consistency requirement can be approximated by the equation [4]

$$\tilde{E}_{refl}(t) = \tilde{E}_{circ}(t - T_{RT}) \times e^{\frac{\delta_m - \delta_c}{2} j T_{RT}(\omega_1 - \omega_0)} \tag{4.1}$$

where *TRT* is the round trip time of the laser cavity, and the factor $\omega_1 - \omega_0$ represents the fact that the circulating and reflected waves oscillate at an optical frequency ω_0.

The condition expressed in Eq. (4.1) is technically only true if the loss and gain factors δ_m and δ_c do not change rapidly during the course of a round trip. In this work we are concerned mainly with the steady state solution to injection locking, and we also restrict our analysis to the case of a weak injected signal. Therefore, Eq. (4.1) is valid for the cases of interest and can be converted to a fairly accurate differential equation, assuming that the frequency detuning between ω_1 and ω_0 is small compared to the axial mode spacing $\Delta\omega_{ax}$, and that the circulating wave does not change severely from one round trip to the next. After solving this differential equation it provides a formula that relates the frequency detuning to the injected wave amplitude and the phase difference between the injected and circulating waves, as given by

$$\omega_1 - \omega_0 = \frac{E_1}{E}\frac{1}{T_{RT}}\sin(\phi_1 - \phi) \tag{4.2}$$

where E_1, ϕ_1 and E, ϕ are respectively the amplitudes and phase of the injected and circular waves. The maximum allowed amplitude of the sine function is 1. Therefore, the maximum detuning is given by

$$\omega_m = \frac{1}{T_{RT}}\frac{E_1}{E} \tag{4.3}$$

This expression gives the maximum allowed detuning between the free-running frequency ω_0 of the laser and the injected frequency ω_1 of the external signal. If the injected frequency is detuned by an amount equal to or less than ω_m, it is said to be within the locking range of the laser. If the amount of detuning is larger than ω_m, injection locking will not occur. Solutions outside the locking range are more complicated and will not be treated in this work.

The regime of interest is those injected frequencies which are within the locking range. Eq. (4.2) indicates that the phase difference between the injected signal and the circulating signal is fixed to a specific value. The phase difference depends on the relative amplitudes of the injected and circulating waves, as well as the amount of the frequency detuning. Rearranging Eq. (4.2), the phase difference is given by

$$\phi_1 - \phi = \sin^{-1}\left[\frac{\omega_1 - \omega_0}{\omega_m}\right] \tag{4.4}$$

From Eq. (4.4), it is clear that as the injected frequency is tuned across the locking range, the phase difference between the injected and circulating waves varies monotonically over a range of π radians, spanning values from $\pi/2$ to $-\pi/2$.

From Eq. (4.3), the maximum detuning ω_m depends on the round trip time and the ratio of the injected and free-running field amplitudes. The field amplitude units can be normalized such that the square of the magnitude of the amplitude represents the power of the wave. The definition of ω_m in Eq. (4.4) is given in terms of the ratio of injected and circulating field amplitudes E_1/E. In terms of power, this is simply the ratio $\sqrt{P_{inj}/P_{circ}}$.This can be translated to a ratio of the incident power and free-running

output power, both of which are waves outside the cavity. Assuming that the injected power is very weak compared to the free-running laser power, the output power from the laser is simply the circulating wave power multiplied by the power transmission coefficient *T* of the input facet. Technically this is the output power from the other laser facet, but in steady state the laser emits the same output at both facets. Therefore, the ratio of injected and circulating field amplitudes is related to the ratio of incident and free running output power by

$$\frac{E_1}{E} = T\sqrt{\frac{P_{inc}}{P_{out}}} = \frac{T}{\sqrt{R}}\sqrt{\frac{P_{inc,refl}}{P_{out}}} \tag{4.5}$$

Experimentally, it is easier to work with the reflected portion of the incident power rather than the total incident power itself.

Figure 4.2: Phase difference $\phi_1 - \phi$ between the injected wave and the injection locked laser output wave, for several values of the power ratio $P_{inc,refl}/P_{out}$.

The phase difference between the incident wave and the injection locked laser output is given by Eq. (4.5), which is expressed in terms of the ratio between the reflected incident power and the free-running laser power. The phase difference $\phi_1 - \phi_0$ is plotted in Figure 4.2 as a function of frequency detuning $\omega_1 - \omega_0$ for power ratios $P_{inc,refl}/P_{out}$, equal to $1/100$, $1/50$, and $1/10$. In each case, the phase difference varies monotonically from $\pi/2$ to $-\pi/2$. For the case of zero detuning, the phase difference is always zero. For each value of the power ratio, the locking range is the range of frequency detuning spanned by the phase difference values. The value of the locking range is equal to $2\omega_m$ because the injected frequency can be detuned both below and above the free-running frequency. The calculated values of the locking range are 2 GHz for a power ratio of 1/100, 3 GHz for a ratio of 1/50 , and 6.5 GHz for a ratio of 1/10.

4.1.1 Diagnostic for Injection Locking

We propose a diagnostic for determining whether the laser is injection locked at a given phase. Fig 4.1 specifically illustrates that on the injection side of the laser, there will be

two signals traveling away from the laser facet. One of the signals is the output of the laser. This output may or may not be injection locked, depending on the injected power and the frequency detuning. The reflected portion of the incident external signal is the second signal which is traveling away from the laser facet on the injection side. The total optical power traveling away from the laser facet is a sum of the electric fields $\tilde{E}_{out}$ of the laser and $\tilde{E}_{inc,refl}$ of the reflected incident signal so the power may be written as

$$P_{out} = \left|\tilde{E}_{out} + \tilde{E}_{inc,refl}\right|^2 \tag{4.6}$$

The signals can be expressed in phasor notation and can be re written as

$$P_{tot} = E_{out}^2 + E_{inc,refl}^2 + 2E_{out}E_{inc,refl}\cos(\phi_{out} - \phi_{inc,refl}) \tag{4.7}$$

The cosine term in Eq. (4.7) indicates that the total power of the signal from the facet strongly depends on the phases of $\tilde{E}_{out}$ and $\tilde{E}_{inc,refl}$. Recall that implicit in this expression is the fact that both $\tilde{E}_{out}$ and $\tilde{E}_{inc,refl}$, are oscillating at the injected frequency ω_1. By definition, $\tilde{E}_{inc,refl}$, is always at ω_1 . However, $\tilde{E}_{out}$ will only be at ω_1 if the laser is injection locked. If it is not injection locked, $\tilde{E}_{out}$ will oscillate at a frequency close to ω_0. This frequency difference would have to be included as a time variation in ϕ_{out}. In this case, the cosine term in Eq. (4.7) would be modulated at the beat frequency $|\omega_1 - \omega_0|$. If this output signal is measured on an optical power meter, the contribution from this modulation term averages out to zero. Therefore, if the laser is not injection locked, the measured total power is simply the sum of the powers of the output and reflected incident waves, as given by

$$P_{out} = E_{out}^2 + E_{inc,refl}^2 \tag{4.8}$$

In other words, the output and reflected incident waves add incoherently if the laser is not injection locked.

The more interesting case occurs when the laser is injection locked. In this case, $\tilde{E}_{out}$ and $\tilde{E}_{inc,refl}$, are both oscillating at ω_1 , and the cosine term in Eq. (4.7) cannot be ignored. The output and reflected incident waves add coherently. Therefore, the coherent interference between the reflected incident wave and the output wave results in a reduction of power compared to the incoherent case. This destructive interference comes

from the two $\pi/2$ phase shifts experienced upon transmission from $\tilde{E}_{inc}$ to $\tilde{E}_{inj}$ and from $\tilde{E}_{circ}$ to $\tilde{E}_{out}$. The amount of interference depends on the phase difference $\phi_1 - \phi$, which is known to depend on the frequency detuning $\omega_1 - \omega_0$ between the injected wave and free-running laser. This destructive interference effect experienced by the output wave on the injection side of the laser is used as a diagnostic for injection locking.

4.2 Mode Locked Laser Fundamentals

Mode-locked lasers are an extremely useful type of laser. The term mode-locking refers to the requirement of phase locking many different frequency modes of a laser cavity. This locking has the result of inducing a laser to produce a continuous train of extremely short pulses rather than a continuous wave (cw) of light. In principle, though, a continuous train of pulses can be generated from a Q-switched laser. The difference between these two scenarios lies in the optical phase of the pulses. The mode locked pulses are phase coherent with each other, while the Q switched pulses are not.

To understand the mode locking process, we will begin by looking at a cw laser in the frequency domain. For a single longitudinal mode cw laser ($\upsilon = c/2nL$ for a Fabry-Perot cavity), we have the situation shown in Fig. 4.3a. Here, only one resonant mode of the laser cavity overlaps in frequency with the gain medium. Thus, the laser emits a cw beam with a narrow range of frequencies($E(t) = E_1 e^{i(w_1 t + \phi_1)}$). In general, however, the gain medium could overlap with several modes. We can describe the output of such a laser in the time domain as:

$$E(t) = \sum_{n}^{N} E_n e^{i(w_n t + \phi_n)} \tag{4.9}$$

where the sum is over all of the lasing cavity modes, E_n is the amplitude of the n^{th} mode, w_n is the angular frequency of the n^{th} mode, and ϕ_n is the phase of the n^{th} mode. For the single-mode laser, this sum just has one term as given above. As we will see, the phase term plays the key role in the difference between incoherent multimode lasing and mode locking.

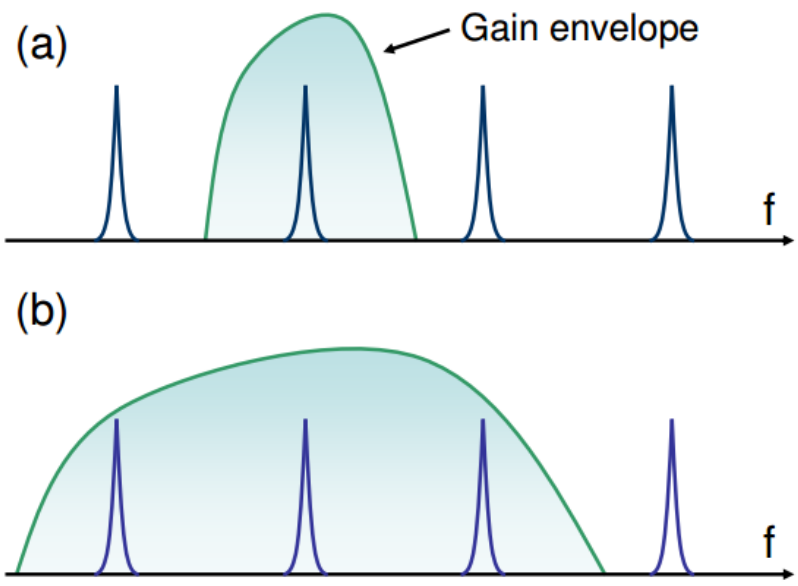

Figure 4.3: Resonant cavity modes and gain spectrum of a laser (a) for single mode lasing (b) for multimode lasing.

If we increase the gain bandwidth to overlap with more of the cavity modes as shown in Fig. 4.3b. In this configuration, there are 3 terms in Eq. 4.9. The output of such a laser depends critically on the phase relationship between the 3 modes. If each mode has a randomly varying phase with respect to the other modes, then a time domain detector on the output would show us that the laser is emitting a cw beam with a large amount of intensity noise (see Fig. 4.4a), while a frequency domain detector would show us that the energy was contained in narrow spikes (with lots of intensity noise) spaced evenly by the free spectral range (FSR) of the cavity. However, if we can fix the relative phases to a set value, then the situation changes dramatically (see Fig. 4.4b and 4.4c). With fixed phase relationships, the three modes can combine to interfere in such a way as to constructively interfere at multiples of the roundtrip time of the cavity, while they destructively interfere elsewhere. This process creates shorter pulses as the number of phase locked modes increases.

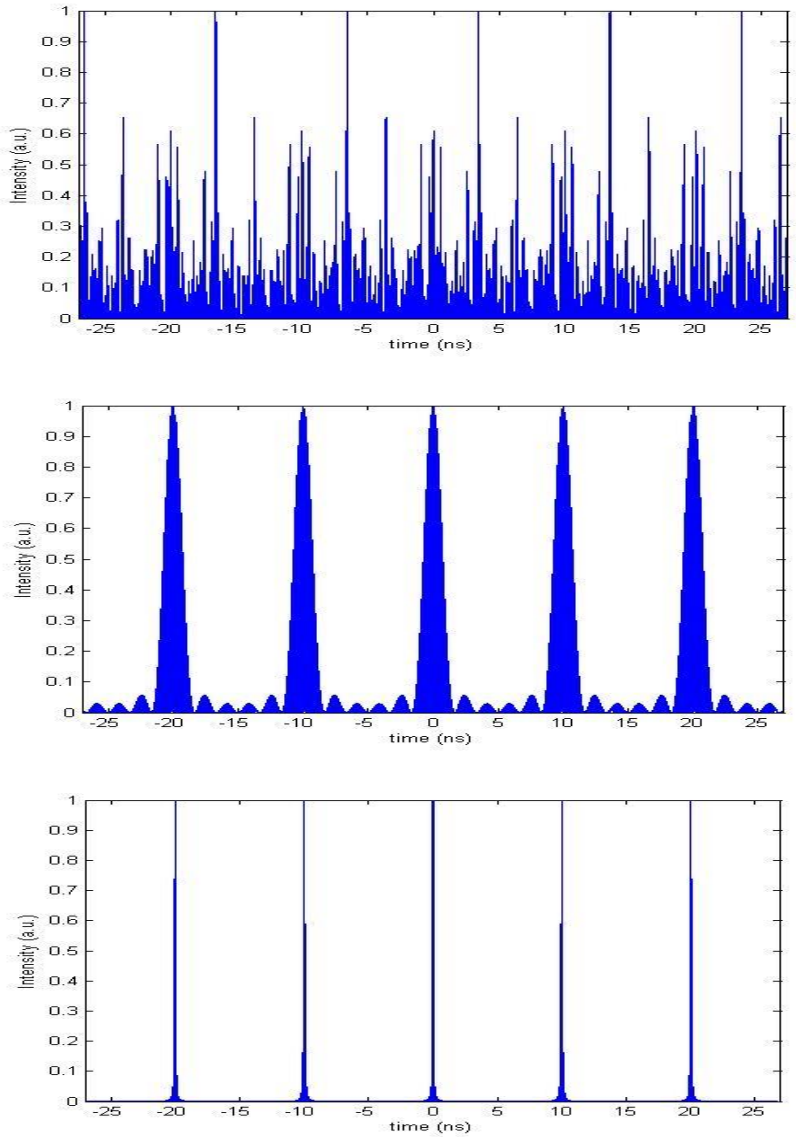

Figure 4.4: Simulation of mode locking. In this simulation, the cavity has FSR = 100 MHz (a) No phase coherence between the multiple modes (80 modes simulated) (b) 5 phase coherent modes (c) 80 phase coherent modes.

A natural question to ponder is exactly how do we achieve this phase locking of the longitudinal modes? We know that a mode-locked laser produces ultrashort pulses at a rate equal to the round trip time of the optical cavity. This means there has to be some part of the laser that prefers to make the laser produce pulses over cw radiation. This statement equates to saying that we need some element that provides high loss at low intensity (cw radiation) and lower loss at high intensity (pulsed operation). Such a device

is known as a saturable absorber. The main feature of the saturable absorber is its decreasing loss with increasing intensity.

4.3 Pulsed Coherent Injection Locking of a Modelocked Laser

The previous sections described mode-locking and injection locking of lasers. This section describes a different method of laser operation which attempts to combine mode-locking and injection locking. A rudimentary numerical model is developed in an attempt to explain the theory. In pulsed injection locking of a mode-locked laser, a pulse train produced by an external laser is injected into an already mode-locked laser. This is similar in some aspects to active or hybrid mode-locking schemes which employ optically-driven modulation of the laser.

In active mode-locking, because the injection and laser signals take the form of pulse trains, the spectra consist of many equally spaced axial modes. It is important to note that this description of the laser spectra assumes that the laser is a linear device. In such active mode-locking schemes with optically-driven modulation, the spectral range of the injection signal is chosen to lie far from that of the free-running modelocked laser. Therefore, there is no coherent interaction between the injection and mode-locked signals. The injected signal only functions to lock the axial mode spacing $\Delta\omega_{ax}$, and therefore the repetition rate, of the mode-locked laser. The injected signal, which has a set RF repetition rate ω_m, modulates the gain of the laser at that rate. This modulation causes the axial modes ω_q of the free-running laser to acquire sidebands at frequencies $\omega_n = \omega_q \pm \omega_m$. If the modulation frequency ω_m is exactly or very closely equal to the free-running axial mode spacing $\Delta\omega_{ax}$, the sidebands ω_n of a given axial mode will lie exactly on or very closely to the neighboring free-running axial modes $\omega_q - n$ and $\omega_q + n$. If the detuning between ω_m and $\Delta\omega_{ax}$ is small enough, then the modulation-induced sidebands will injection lock the neighboring free-running axial modes, in a process much like CW injection locking. This locks the axial mode spacing $\Delta\omega_{ax}$ of the laser to the RF frequency ω_m of the injection signal. This process is illustrated in Fig. 4.5. It is important to note that although the sidebands are

induced by the injection signal, their phases do not depend on the injection. In standard active mode-locking, the goal is to produce a pulsed signal with a fixed repetition rate.

Pulsed coherent injection locking differs from optically-driven active modelocking in that it uses an injection signal whose spectral range is purposefully chosen to overlap with that of the free-running laser. This is illustrated in Fig. 4.6. In this case, the modes of the injected signal themselves may, under proper conditions, injection lock the free-running axial modes of the laser. Therefore, not only does the repetition rate of the laser become locked to that of the injection signal, but the phases of the laser axial modes depend directly on the phases of the injected signal modes. Consider an injection signal that possesses modes with a very well-defined phase relationship. The mode-locked laser will obtain this desirable phase relationship through the injection locking process. Thus, the proposed method aims to achieve both mode-locking and coherent injection locking of a free-running laser using a high quality mode-locked injection signal.

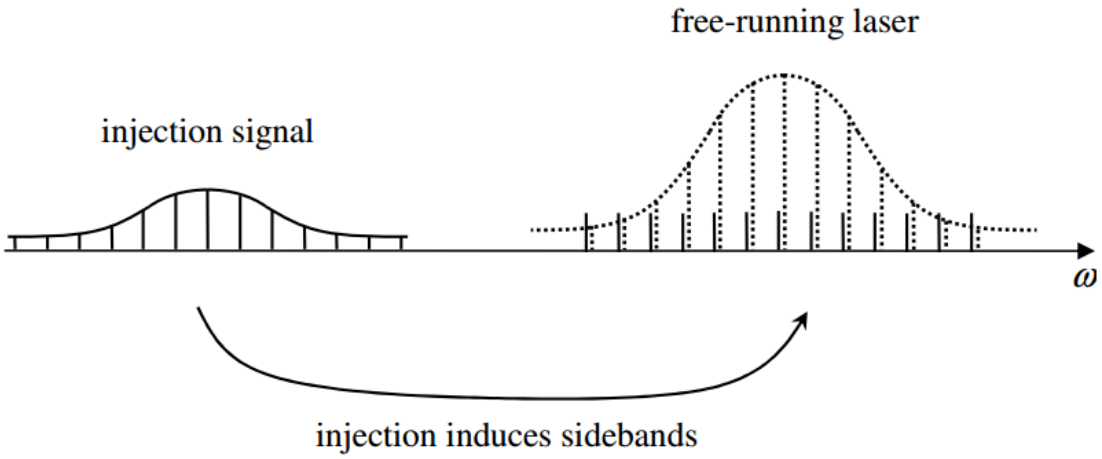

Figure 4.5: Illustration of optically driven active mode locking

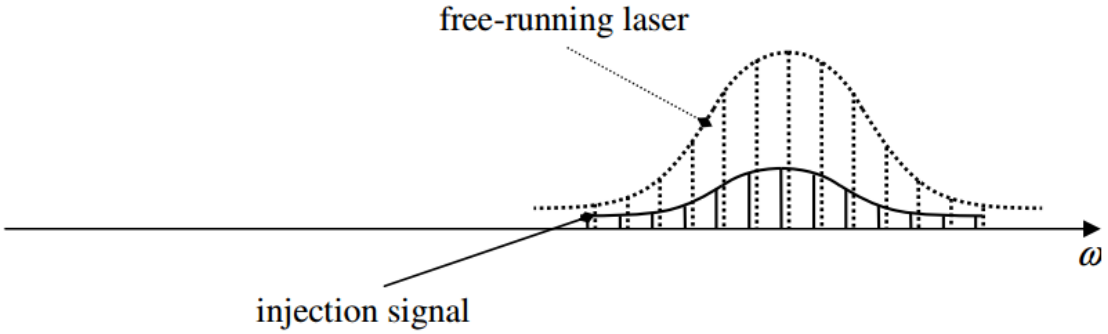

Figure 4.6: Illustration of Pulsed coherent injection locking

Pulsed coherent injection locking of a mode-locked laser requires two criteria be met. First, the detuning between the injection laser repetition rate and the free-running laser repetition rate must be small enough such that active mode-locking occurs. In other words, the mode spacing ω_m of the injected signal must be close enough to the mode spacing $\Delta\omega_{ax}$ of the free-running laser. This is the same requirement as for standard active mode-locking. Second, the actual locations of the injected modes in frequency must lie very close to the locations of the free-running axial modes. This is the same requirement as for CW injection locking. In order to achieve pulsed injection locking of a mode-locked laser, the characteristics of the injection signal or the free-running laser must be adjusted to meet these criteria. It is important to note that the pulsed coherent injection locking method involves using a free-running laser which is already mode-locked by passive modelocking techniques. The passively mode-locked laser utilizes the nonlinearity of the saturable gain and saturable absorber sections. In the presence of the strong nonlinearity, the axial modes of the free-running laser are not as simply defined as in the case of a linear system. The round-trip time *TRT* of the laser pulse circulating in the laser does not simply depend on the cavity length and the index of refraction of the medium. The nonlinearities cause the effective refractive index to change rapidly in time. Pulse reshaping due to the saturable gain and absorption changes the effective round-trip time in a way which is difficult to quantify. As a result, the repetition rate also depends on the saturation dynamics in a complicated way. Therefore, the so-called axial modes of the free-running laser exist only in steady state operation, and are determined by a complicated process.

4.4 Numerical Model

A simple numerical model was developed in an attempt to explain the theory of the pulsed injection locking method. The model treats the Self Colliding Pulse Mode locked Laser (SCPM) laser as the combination of a saturable gain section, a saturable absorber section, an unsaturable absorption factor, and a bandwidth limiting element. It includes the key effect of tuning of the SCPM laser cavity. In addition, it takes into account the fact that the true repetition rate of the laser output does not correspond to the physical length of the laser cavity. A schematic of the model is shown in Fig.4.7. The model is exceedingly rudimentary, and requires much more development. However, it is capable of qualitatively confirming two of the effects. First, the reflected power diagnostic for injection locking introduced in Section 4.1.1 is generated by the model. Second, the shifting behavior of the output optical spectrum is also exhibited in the numerical results.

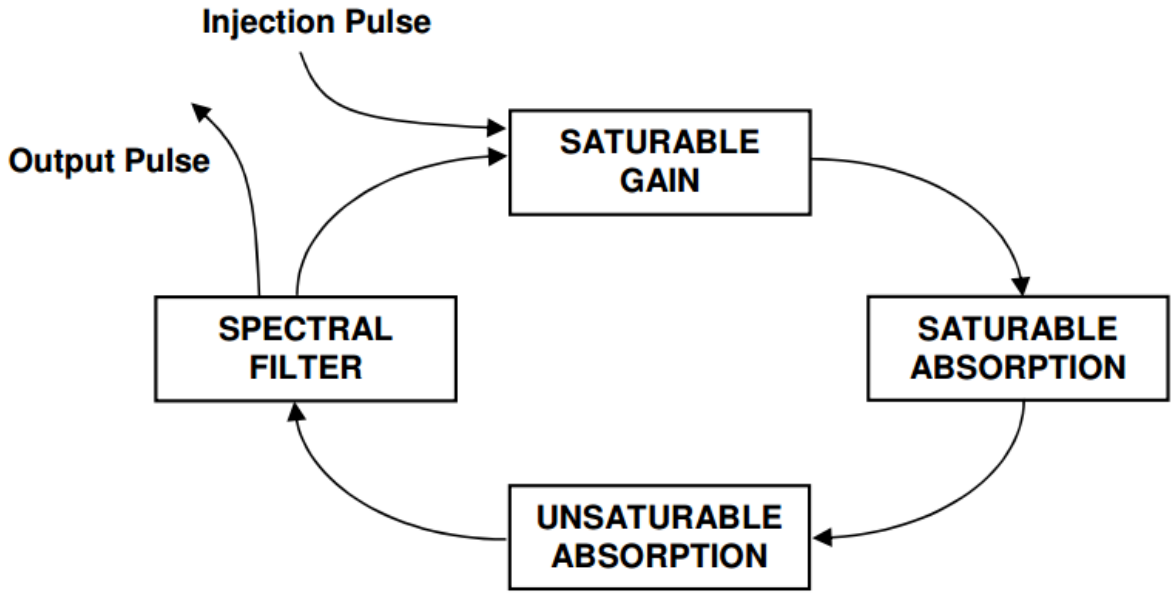

Figure 4.7: Schematic of numerical model for pulsed injection locking of a mode locked laser

The structure of the model follows a loop which is repeated until the calculated laser signal reaches a steady state. On each round trip, the model starts with an electric field

phasor $E_1[t]$ which is defined over a time array t. The time array spans a period of 100ps, which corresponds to a cavity round trip time of 10 GHz. The time step dt of the time array is 0.1 ps. The FrantzNodvik equation is used to calculate the time-varying gain that the saturable gain element applies to $E_1[t]$. The equation is given from Section 2.2.1,

$$G[t] = \frac{G_0}{G_0 - (G_0 - 1)e^{-\frac{U_1[t]}{E_{sat,G}}}} \tag{4.10}$$

where $E_{sat,G}$, is the saturation energy of the saturable gain element, and G_0 is the unsaturated value of the gain. By using the same constant value for the unsaturated gain on every round trip, the model assumes that the gain recovers fully after each round trip. Here, $U_1[t]$ is the integrated cumulative energy in $E_1[t]$, and is given by

$$U_1[t] = \frac{1}{2}\left\{I_1[1] + I_1[t] + 2\sum_{m=2}^{t-1} I_1[m]\right\} \times dt \tag{4.11}$$

Here, $I_1[t] = |E_1[t]|^2$ is the intensity associated with $E_1[t]$. The integration of the intensity is numerically calculated using the trapezoid rule. Once the integrated energy and gain are calculated, the gain is applied to $E_1[t]$, and the result is named $E_2[t]$. The resulting field is

$$E_2[t] = e^{g/2 \times -j\alpha_G g/2} \times E_1[1] \tag{4.12}$$

Here, $g = \ln(G)$ is the exponential gain coefficient and α_G is the linewidth enhancement factor of the saturable gain section. Next, the effect of the saturable absorber is calculated in the same way as that of the saturable gain. The saturable absorption is simply

$$A[t] = \frac{A_0}{A_0 - (A_0 - 1)e^{-\frac{U_2[t]}{E_{sat,A}}}} \tag{4.13}$$

where $E_{sat,A}$, is the saturation energy of the saturable absorber, and A_0 is the unsaturated value of the absorption. As with the saturable gain, the model assumes that the saturable absorber recovers fully after each round trip. The cumulative energy $U_2[t]$ is calculated in the same way as for $U_1[t]$. The resulting field $E_3[t]$ after the saturable absorber is given by

$$E_3[t] = e^{a/2 \times -j\alpha_A a/2} \times E_2[t] \tag{4.14}$$

The unsaturable absorption is simply modeled by a constant power loss coefficient K. It takes into consideration the cavity losses due to the portions of the circulating laser energy which transmit out of the cavity on each round trip, as well as any intrinsic losses inside the cavity. The field after the unsaturable absorption is

$$E_4[t] = \sqrt{k} \times E_3[t] \tag{4.15}$$

where the square root is due to the fact that k represents the power loss.

Next, a bandwidth limiting element is included to account for the fact that the actual laser gain has a finite spectral width. Indeed, this spectral filter component is critical for the model to function properly. Without the spectral filter, the saturable gain and absorption dynamics work to narrow the circulating laser pulse on each round trip. The finite bandwidth of the laser limits the ultimate pulse narrowing that can be achieved. The effect of the spectral filter is calculated by first taking the Fourier transform of the field $E_4[t]$, which is denoted by $\tilde{E}_4[t]$, and then applying a Gaussian filter in the frequency domain, given by

$$\tilde{E}_5[f] = \tilde{E}_4[f] \times e^{-4\ln(2)(f/w)^2} \tag{4.16}$$

where w is the FWHM of the spectral filter in Hz. The inverse Fourier transform of the resulting spectrum $\tilde{E}_5[f]$ is then taken to yield the circulating signal $E_5[t]$.

Then, the effect of the cavity tuning is calculated. When the laser cavity is tuned by adjusting the pumping current, the axial modes ω_q are shifted by a small amount. This is equivalent to applying a small, constant phase change θ to the circulating laser signal. If the axial modes are shifted by an amount equal to the axial mode spacing $\Delta\omega_{ax}$, which results in the shift of any given mode ω_q to its adjacent neighbor ω_{q+1} , the associated constant phase change experiences a variation from 0 to 2π. Therefore, the effect of cavity tuning is calculated by

$$E_6[t] = E_5[t] \times e^{j\theta} \tag{4.17}$$

The value of θ is varied from 0 to 2π to simulate change in cavity tuning that results in a spectral shift of $\Delta\omega_{ax}$. On each round trip, the circulating signal is also assumed to shift in time by a constant δt. This takes into consideration the fact that the true repetition rate of the laser does not depend simply on the cavity length and background refractive index. As mentioned earlier, the nonlinearities of the laser cause the true repetition rate to settle to a value different from that of the ideal cold cavity. If the time shift δt is not included, the pulse becomes shifted within the time window by a small amount from each round trip to the next. By incorporating the time shift, we are slightly shifting the time window on each round trip. As a result, the repetition rate of the injection signal is different from the cold cavity round trip. This time shift correction is calculated by employing the Fourier transform duality rule which states that a shift in time domain is equivalent to a linearly varying phase in frequency domain. The field $E_6[t]$ is transformed to Fourier domain, then multiplied by a linearly varying phase in frequency, and the resulting field $\tilde{E}_7[f]$ is transformed back to the time domain. The calculation is given by

$$\tilde{E}_7[t] = \tilde{E}_6 \times e^{-j2\pi f \delta t} \tag{4.18}$$

The resulting circulating field $E_7[t]$ is then redefined as $E_1[t]$, and the process is repeated for successive round trips. The inclusion of this time shift factor, combined with the fact that the injected pulse is always placed in the center of the time window, means that the injection signal has an actual repetition rate that is different from the 10 GHz rate that corresponds to the 100ps time window. Effectively, it is the injection signal that deviates from the 10 GHz rate. Since the inclusion of the time shift factor results in stable solutions for some values of θ , we assume that for these conditions, the injected signal is matched to the natural repetition rate of the free running laser. This natural repetition rate is difficult to calculate, as it depends in a complicated way on the saturation dynamics of the laser. On each round trip, the coherent interference effect between the reflected incident signal and the output of the laser from the input facet is calculated. The total interfered signal $E_{reduc}[t]$ is given by

$$E_{reduc}[t] = \tau \times E_1[t] + \rho \times E_{inc}[t] \tag{4.19}$$

where τ is the complex field transmission coefficient of the cavity facet and ρ is the reflection coefficient. The injected signal $E_{inj}[t]$ is simply given by the incident signal $E_{inc}[t]$ multiplied by τ. On each round trip, the new circulating signal $E_1[t]$ is augmented by adding $E_{inj}[t]$. A running average of the total energy of $E_{reduc}[t]$ is calculated on each round trip. For a given value of the cavity tuning θ, this average energy represents the amount of interference on the injection side of the laser. This is the coherent injection diagnostic described in Section 4.1.1.

The model is run for different values of cavity tuning θ, over a range of 2π radians to represent shifting of the laser axial modes over an amount equal to the axial mode spacing. For each value of θ, the model is run until either the circulating pulse stabilizes to an unchanging shape, or until an arbitrary maximum number of round trips has been reached. In order to keep the runtime of the program manageable, the model is allowed to run up to 50 round trips before the system is deemed unstable for the particular value of θ. Using this criterion, it is found that the system is only stable over a narrow range of cavity detuning θ. We assume that a stable output corresponds to the case of coherent injection locking.

It is assumed that the model is only valid for values of cavity tuning within the injection locking range, which occurs in the region of reduced power. Outside this range, we expect that the laser will not be injection locked. Indeed, the model only yields stable solutions for values of θ between $-0.44 \times 2\pi$ and $-0.29 \times 2\pi$. This is due to the fact that outside the injection locking range, the laser essentially operates in its free-running SCPM regime or in the active mode-locked regime. Unfortunately, the model does not incorporate the effects necessary to simulate this regime of operation. The model uses reasonable values for the various constants in the equations. The cavity facet field reflection and transmission coefficients are set to $\rho = 0.6$ and $\tau = j \times 0.8$. These are chosen based on the typical refractive index difference at an air-to-semiconductor interface. Also, ρ and τ are offset by a constant phase of $\pi/2$, by making ρ purely real and τ purely imaginary, to account for the transmission effect discussed in Section 4.1.1. The unsaturated gain and absorption values are set to $G_0 = e^3$ and $A_0 = e^{-0.1}$, respectively. The linewidth enhancement factors α_G and α_A for the saturable gain and

absorber sections are both set to 3. The energy of the gain section is, $E_{sat,G} = 1$ pJ, while the saturation energy of the absorber section is, $E_{sat,A} = 0.2$ pJ. The ratio of the saturation energies $E_{sat,G}/E_{sat,A} = 5$ is typical for semiconductor mode-locked lasers [5].The bandwidth of the Gaussian spectral filter is $w = 5 \times 10^{11}\ Hz$. The unsaturable loss factor is $K = 0.1$. The incident wave energy is $E_{inc} = 0.5\ pJ$. The repetition rate correction time is $= 1.5\ ps$ s , which corresponds to a deviation of about 152 MHz from the 10 GHz cavity repetition rate.

4.4.1 Simulation Results

The value of the reflected power is calculated as a function of the cavity tuning, expressed in terms of θ, and is shown in Fig.4.8. This agrees qualitatively with the theory introduced in Section 4.1.1. The simulated curve exhibits the reduced power due to coherent injection.

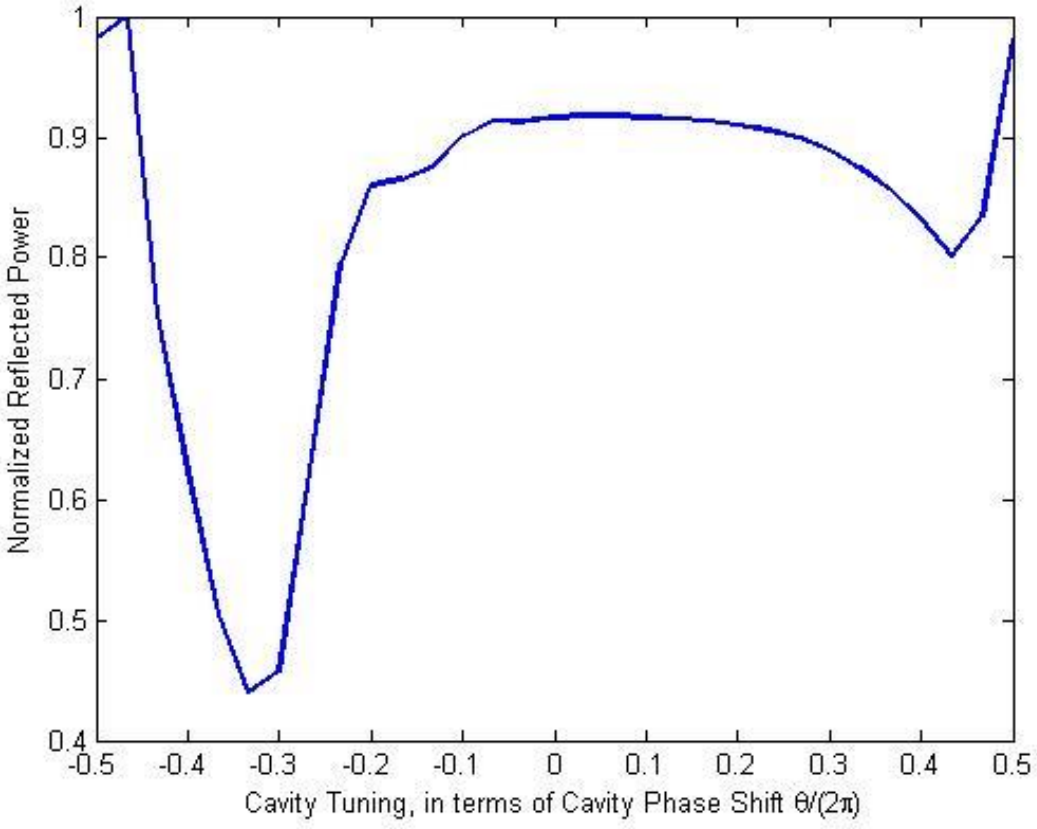

Figure 4.8: Simulated reflected power from the laser cavity

In Fig.4.9, the calculated laser output spectrum is plotted for various values of the cavity round trip phase detuning. According to the model, only the narrow range of values from $-0.44 \times 2\pi$ to $-0.29 \times 2\pi$ yield stable solutions. These solutions reach a steady state after less than 50 round trips, and are plotted as solid, bold curves. The plotted spectra in the range of unstable solutions continue to fluctuate even as the number of round trips is increased. The unstable spectra are not an accurate depiction of the real laser system outside the locking range. Therefore, they are plotted as dashed, thin curves to represent the fact that significantly more work is needed to accurately model this regime.

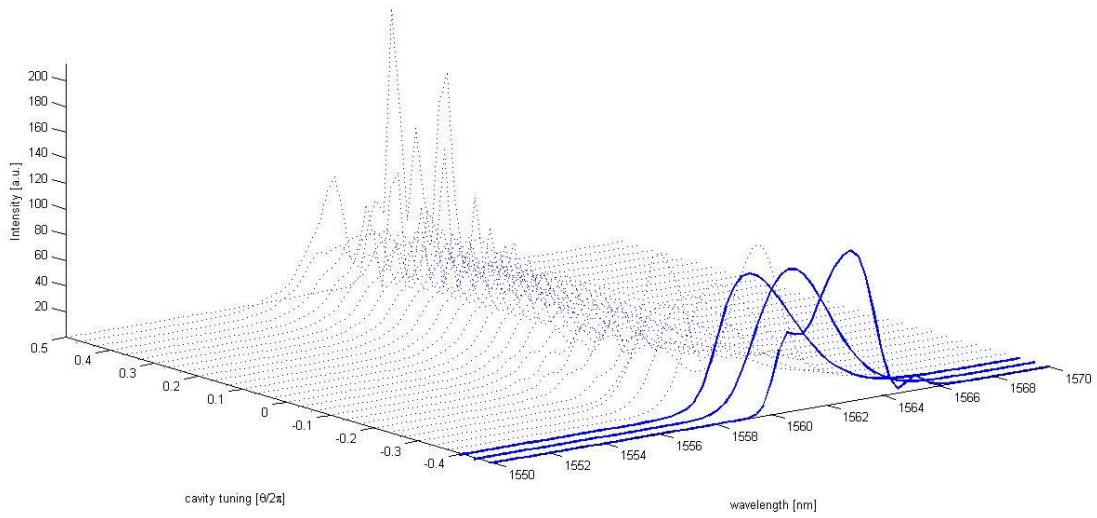

Figure 4.9: Simulated laser spectra for various values of θ

Several selected laser spectra, for values of θ equal to $-0.44 \times 2\pi$, $-0.36 \times 2\pi$, and $-0.29 \times 2\pi$, are shown in Fig.4.10. As the cavity round trip phase is tuned across the coherent injection locking range, in the direction of increasing pumping current, the peak of the spectrum shifts from higher wavelengths to lower wavelengths. The simulated spectral peak shifts from 1561.6 nm at $\theta = -0.44/2\pi$ to 1558.6 nm at $\theta = -0.29/2\pi$, which is a 3 nm shift. Therefore, the model confirms the spectral shift behavior of the laser.

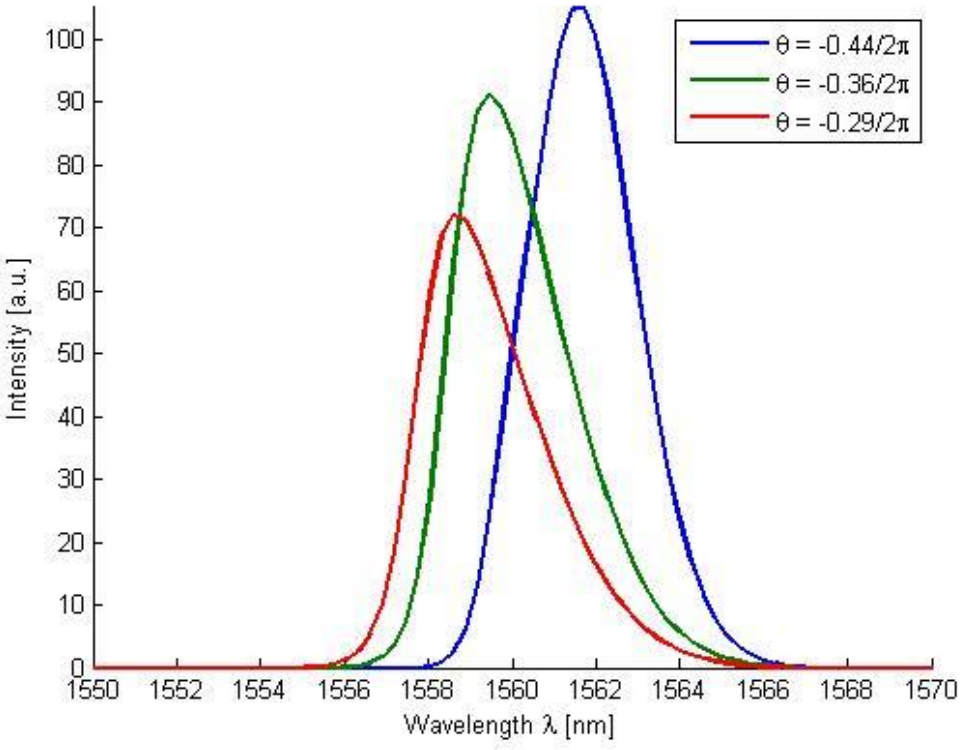

Figure 4.10: Selected simulated laser output spectra, for values of θ within the coherent locking range. A shift in the peak of the spectrum occurs as θ is tune

The simulated laser pulses for various values of θ across a full range of 2π are presented in Fig.4.11. In the model, the injected pulse that is added on each round trip is centered around 50 ps. This is the center of the time window used in the model. The few pulses which are shown within the coherent injection locking range are centered near 50 ps, which is expected for coherent locking. The pulse-like solutions which are plotted for θ outside the coherent locking range are unstable solutions. The simulation was arbitrarily run for 50 round trips. If the simulation is continued for more round trips, the pulses in the unstable region will continue to shift in position in the time window, as well as undergo dramatic changes in pulse shape. However, the pulses in the coherent locking range remain unchanged if the simulation is continued for more round trips.

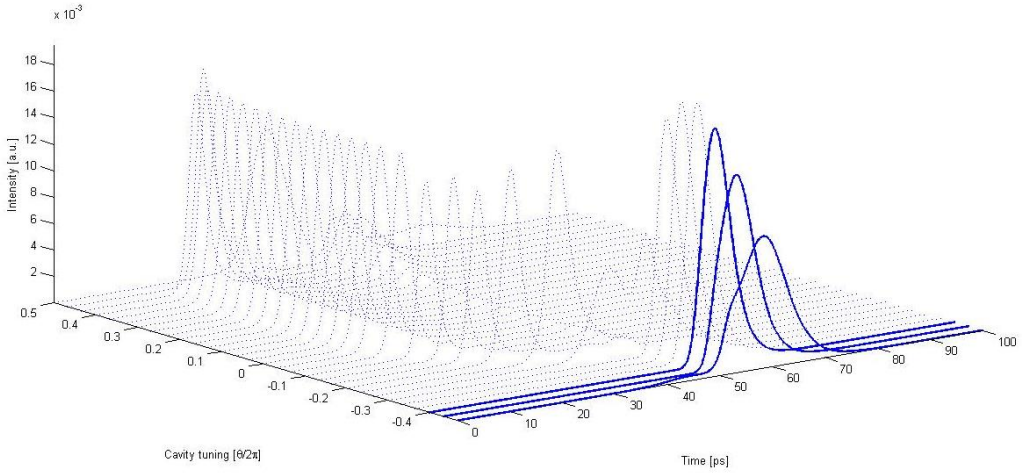

Figure 4.11: Simulated laser pulses for various values of θ.

Several selected laser pulses, for values of θ equal to $-0.44/2\pi$, $-0.36/2\pi$, and $-0.29/2\pi$, are shown in Fig.4.12. Pulse-like solutions are obtained, with FWHM ranging from 8.8ps at $\theta = 0.44/2\pi$ to 4.6 ps at $\theta = -0.29/2\pi$. The peak of the pulse shifts from about 56.4ps at $\theta = -0.44/2\pi$ to about 53.1 ps at $\theta = -0.29/2\pi$. Therefore, the pulse seems to advance in time by about 3.3ps as the cavity round trip phase θ is tuned across the coherent injection locking range.

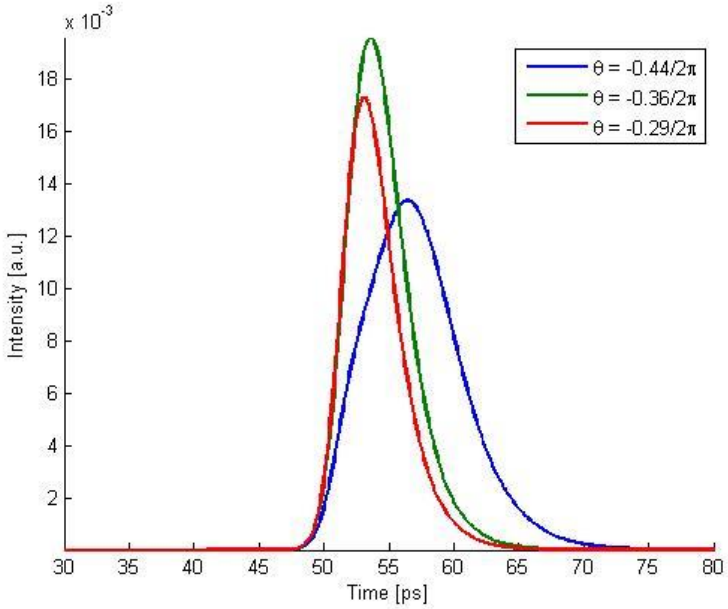

Figure 4.12: Selected simulated laser pulses for values of θ within the coherent injection locking range.

4.5 Conclusion

In summary, the simple model provides qualitative support for the spectral shift of the laser pulse under locking condition. However, the model in its current state cannot quantitatively explain the laser system. The pulsed injection locked laser works by the interaction between the free-running laser signal and an injection signal. The model merely attempts to simulate the effects of the laser on a circulating signal. In steady state coherently locked operation, this circulating signal is assumed to primarily depend on the injection signal. The model does not simulate the free running laser, and therefore the critical interaction is not included.

The simple theoretical model presented in this chapter requires much more work to accurately describe the proposed method of pulsed coherent injection locking of a mode-locked laser. As presented, the model assumes reasonable values for the unsaturated gain and absorption, linewidth enhancement factors, gain and absorption saturation energies, laser facet reflectivity and transmission, unsaturable loss, and the bandwidth of the spectral limiting element. In addition, the model neglects several potentially important effects. Most obviously, the model does not simulate the free-running laser. It merely examines the situation that results when a period pulse train is injected into the system. This neglects the complicated interaction between the injected and free-running signals. In addition, group velocity dispersion is not taken into account. Also, in using the Frantz-Nodvik relation, it is assumed that the saturable gain and absorption fully recover on each round trip. A more precise treatment would consider the effects of gain and saturation recovery. Therefore these concepts can be clearly used for All-Optical Clock recovery solutions where the injected laser (master) can send the data and the free running mode locked laser (slave) can act as optical clock source which is tuned and synchronized by the master laser.

BIBLIOGRAPHY

[1] A. E. Siegman, *Lasers* (University Science Books, Sausalito, 1986)

[2] T. von Lerber, S. Honkanen, a. Tervonen, H. Ludvigsen, and F. Kuppers, "Optical clock recovery methods: ¨ Review (Invited)," Optical Fiber Technology **15**, 363–372 (2009).

[3] B. Razavi, "Monolithic phase-locked loops and clock recovery circuits, theory and design," IEEE press, 1996

[4] X. Wang, H. Yokoyama, and T. Shimizu, "Synchronized Harmonic Frequency Mode-Locking with Laser Diodes through Optical Pulse Train Injection," IEEE Photon. Technol. Lett., 8, 617-619 (1996).

[5] R.G.M.P. Koumans and R. van Roijen, "Theory for Passive Mode-Locking in Semiconductor Laser Structures Including the Effects of Self-Phase Modulation, Dispersion, and Pulse Collisions," IEEE J. Quantum Electron., 32, 478-492 (1996).